THEORY OF LOW FREQUENCY WAVES IN A ROTATING STRATIFIED CHANNEL

by

John Arthur Vermersch, Jr.

B.S., North Texas State University

(1972)

SUBMITTED IN
PARTIAL FULFILLMENT
OF THE REQUIREMENTS FOR THE
DEGREE OF MASTER OF SCIENCE

at the

MASSACHUSETTS INSTITUTE OF TECHNOLOGY

August, 1974

Signature of Author _____

Department of
Meteorology
August 12, 1974

Certified by _____

Thesis Supervisor

Accepted by _____

Chairman, Department Committee
on Graduate Students

Theory of Low Frequency Waves In a Rotating Stratified Channel

by
John Arthur Vermersch, Jr.

Submitted to the Department of Meteorology on August 12, 1974 in partial fulfillment of the requirements for the degree of Master of Science.

ABSTRACT

It is found that the possible low-frequency, quasigeostrophic motions in a rotating and stratified channel with a wavemaker at one end include: (i) standing waves whose amplitudes are damped exponentially away from the forcing, and (ii) baroclinic internal Kelvin waves, trapped to the right hand wall when facing in the direction of phase propagation. The Kelvin waves are excited only if the wavemaker transfers mean energy to the fluid. The standing waves, on the other hand, carry no energy and thus serve mainly to provide continuity between the wavemaker and the fluid.

When the bottom of the channel is inclined to the horizontal by a small angle α, topographic oscillations are possible. These waves behave like topographic Rossby waves if the forcing frequency is greater than SN and if the ratio $\frac{HN}{fL}$ is small. S is $\tan\alpha$, L is the width of the channel, H is the mean depth, f is the Coriolis parameter and N is the Brunt-Vaisala (or buoyancy) frequency. It is determined that topographic Rossby waves cannot exist in the channel if $HN/fL \gtrsim .22$.

If the wavemaker frequency is smaller than SN, and if $\frac{HN}{fL} \sim O(1)$, the topographic oscillations become bottom-trapped, decaying away from the bottom boundary in a distance of $O(Kf/HN)$, where K is the horizontal wave length. The phase and energy of the bottom-trapped wave both move to the left of an observer who is facing shallow water. The standing oscillations of the flat-bottom case exist as complex horizontal wave number solutions to the topographic wave dispersion relation. Although these waves have propagating phase when $S \neq 0$, they are still trapped to the forcing, and do not transfer net energy from the wavemaker to the fluid.

The Kelvin waves are basically unchanged when the bottom is sloped if their down-channel wave length is large relative to the slope parameter $\epsilon = \frac{SL}{H}$.

A laboratory experiment to isolate and study the bottom-trapped waves in such a channel is devised and experimental parameters are chosen.

Thesis Supervisor: R.C. Beardsley
Title: Associate Professor of Oceanography

ACKNOWLEDGEMENTS

The author is indebted to Dr. R. C. Beardsley for the support he has given while this work was in progress.

This work was supported by the U.S. Office of Naval Research, N00014-67-A-0204-0048, and by the National Science Foundation, NSF-GA-41073.

TABLE OF CONTENTS

Page

Chapter I Introduction

Rhines (1970) first studied the quasigeostrophic theory for oceanic flow including the effects of both topography and continuous stratification. He predicted the existence of bottom-trapped internal waves, which are essentially buoyancy waves (of frequency $\sigma \leq N \sin\theta$, where θ is the inclination angle of the bottom away from horizontal) trapped near the bottom boundary. In the low frequency limit ($\sigma \ll f$, $\sigma \ll N$), these wave modes decay exponentially away from the boundary with a decay length of $O(\frac{f}{N}K)$ where f is the Coriolis parameter, N is the Brunt-Vaisala (or buoyancy) frequency, and K is the horizontal wave length. Rhines found that these bottom-trapped waves exist as eigenmodes in a linearly stratified fluid for a number of special geometries.

Suarez (1971) next investigated the way in which these low frequency topographic oscillations propagate and are generated over topography. He found that Rossby waves do not efficiently excite bottom-trapped waves, but rather excite other topographic modes with a horizontal (and thus vertical) velocity node on the bottom boundary surface. Suarez also found that when the scales of an initially imposed disturbance are smaller than $\frac{NH}{f}$, where H is the mean depth, the resulting motions consist of a steady current and the bottom-trapped wave. Suarez shows that the only part of a steady geostrophic flow affected by a region of sloping bottom is the part of the flow which comes in contact with the bottom. The steady flow develops a velocity node on the bottom, and the bottom-trapped waves are induced to transport the "bottom energy" of the

initial flow. Suarez suggests that this is the most important role of bottom-trapped waves -- to release the ocean interior from the constraints imposed by topography.

Although there are many ocean regions in which the horizontal scale of the observed motion is smaller than $\frac{HN}{f}$, bottom-trapped waves have not been directly observed. There is, however, observational evidence which indicates that motion is intensified toward the bottom. Riser (1974) reviews the attempts to explain bottom-intensification, and presents data from the MODE-O experiment which confirms the intensification of motion with depth over sloping regions. Riser shows that the data may not be inconsistent with the bottom-trapped wave theory of Rhines.

A laboratory experiment designed to isolate and study bottom-trapped waves would be very useful in confirming the existing theory of bottom-trapped waves and perhaps provide more insight into their role in the ocean. It was decided to model the waves in a long channel because of the simple geometry and the simplicity of forcing the fluid with a wavemaker.

This thesis examines the possible wave motions in a rotating and continuously stratified channel, and proposes an experiment designed to isolate bottom-trapped oscillations in the laboratory. The thesis is organized as follows: a theoretical study of the wave motions allowed in the channel is made in Chapter 2, the wavemaker problem (matching the fluid modes to a specified forcing in one end of the channel) is outlined in Chapter 3, and finally, Chapter 4 describes the laboratory experiment designed to isolate and study bottom-trapped waves.

Chapter II Wave Motion In A Rotating-stratified Channel.

In this chapter, the low-frequency wave modes for the semi-infinite channel (Figure 1) will be examined. The vertical coordinate is Z, the cross-channel coordinate is Y and the along-the-channel coordinate is X. The channel sidewalls are at $Y=0$ and $Y=L$, and the top is at $Z=H$. The bottom, inclined slightly away from the horizontal by the angle α, is at $Z=SY$, where S is defined as $\tan\alpha$. We will examine the fluid response to a general forcing applied at $X=0$, and will consider motion only to the left of an observer at the origin who is facing in the $+Y$ (upslope) direction.

The linearized, inviscid Boussinesq equations are

(2.1) $\frac{\partial \vec{u}}{\partial t} + 2\vec{\Omega}\times\vec{u} = -\nabla P - g\rho\hat{k}$ (momentum equation),

(2.2) $\nabla\cdot\vec{u}=0$ (continuity equation), and

(2.3) $\frac{\partial \rho}{\partial t} - \frac{N^2\vec{u}\cdot\hat{k}}{g} = 0$ (equation of incompressibility).

$\hat{k}$ is the vertical unit vector, $\vec{\Omega}$ is the rotation vector $\Omega\hat{k}$, and $\vec{u}$ is the fluid velocity vector (u, v, w). The density is written $\rho_T = \rho_0(1+\rho_1(z)+\rho(x,y,z,t))$. ρ_0 is the mean density, $\rho_1(z)$ is the deviation from the mean due to the initially imposed stratification, and $\rho(x,y,z,t)$ is the density deviation due solely to the fluid motion. P is the deviation from hydrostatic pressure divided by the mean density ρ_0; however, P

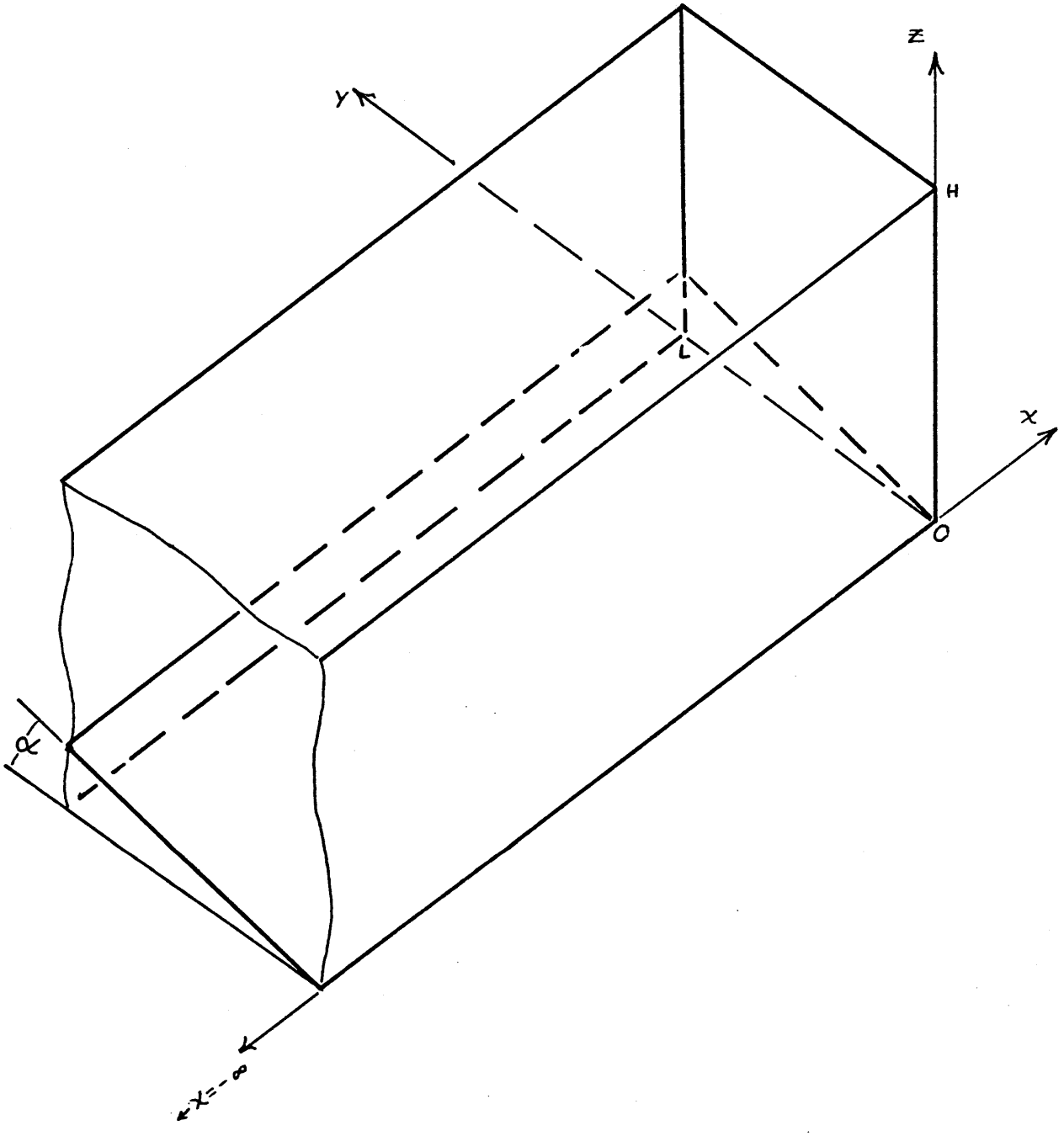

Figure 1.

Geometry of the Channel.

will henceforth be referred to as simply "pressure" . N is the Brunt-Vaisala (buoyancy) frequency ($N^2 \equiv -\frac{g}{\rho_0}\frac{\partial \rho_1}{\partial z}$) which we assume will be constant, and g is the gravitational acceleration.

In component form, the equations are

(2.4) $u_t - fV = -P_x$,

(2.5) $V_t + fu = -P_y$,

(2.6) $W_t + \rho g = -P_z$,

(2.7) $u_x + V_y + W_z = 0$, and

(2.8) $\rho_t - \frac{N^2 W}{g} = 0$, where $f = 2\Omega$.

The boundary conditions are

(2.9) $W = 0$ at $z = H$,

(2.10) $V = 0$ at $y = 0, L$ and

(2.11) $W = SV$ at $z = Sy$.

In addition to these explicit boundary conditions, we also demand

that none of the variables P, $\vec{u}$, ρ grow without bound as $|x| \to \infty$. After the possible modes of oscillation are determined, we complete the problem by matching the fluid to a forcing function at $x = 0$ (wavemaker problem).

We first separate the time dependence from the spatial dependence by writing

$$\text{(2.12)} \quad \begin{bmatrix} u \\ v \\ w \\ p \\ \rho \end{bmatrix} = Re\left[\begin{pmatrix} u' \\ v' \\ w' \\ p' \\ \rho' \end{pmatrix} e^{-i\sigma t} \right] .$$

The equations become (dropping primes):

$$\text{(2.13)} \quad i\sigma u + fv = p_x \quad ,$$

$$\text{(2.14)} \quad i\sigma v - fu = p_y \quad ,$$

$$\text{(2.15)} \quad i\sigma w - \rho g = p_z \quad ,$$

$$\text{(2.16)} \quad i\sigma \rho + \frac{N^2 w}{g} = 0 \quad , \text{ and}$$

$$\text{(2.17)} \quad u_x + v_y + w_z = 0 \quad .$$

Eliminating ρ from (2.15) and (2.16) yields

$$\text{(2.18)} \quad w = \frac{i\sigma p_z}{N^2 - \sigma^2} \quad .$$

We use the horizontal momentum equations (2.13 and 2.14) to express u and v in terms of the pressure:

(2.19) $u = -\frac{1}{f^2-\sigma^2}(fP_y - i\sigma P_x)$, and

(2.20) $v = \frac{1}{f^2-\sigma^2}(fP_x + i\sigma P_y)$.

Substituting 2.18, 2.19, and 2.20 into the continuity equation (2.17) and the boundary conditions, we arrive at

(2.21) $P_{xx} + P_{yy} + \frac{f^2-\sigma^2}{N^2-\sigma^2}P_{zz} = 0$, with the boundary conditions

(2.22) $P_z = 0$ at $z = H$,

(2.23) $fP_x + i\sigma P_y = 0$ at $y = 0, L$, and

(2.24) $i\sigma\left(\frac{f^2-\sigma^2}{N^2-\sigma^2}\right)P_z = S(fP_x + i\sigma P_y)$ at $z = Sy$.

We now scale x and y by the width of the channel (L), and scale z by the zero-slope height (H). After scaling, the governing equation becomes

(2.24) $P_{xx} + P_{yy} + B^2 P_{zz} = 0$, with the boundary conditions

(2.25) $P_z = 0$ at $z = 1$,

(2.26) $P_x + i\delta P_y = 0$ at $y = 0, 1$, and

(2.27) $i\delta B^2 P_z = \epsilon(P_x + i\delta P_y)$ at $z = \epsilon y$.

The non-dimensional parameters appearing in 2.24 - 2.27 are defined as follows:

$$\delta = \frac{\sigma}{f} ,$$

$$B^2 = \frac{f^2 - \sigma^2}{N^2 - \sigma^2}\left(\frac{L}{H}\right)^2 , \text{ and}$$

$$\epsilon = \frac{S}{H/L} .$$

We first solve for the case of a flat-bottom ($\epsilon = 0$) channel. In this case the bottom boundary condition (2.27) becomes

(2.28) $P_z = 0$ at $z = 0$, and together with 2.25, this requires that the vertical structure be $\cos s\pi z$, $s = 1, 2, 3, \ldots$.

If we separate the remaining variables by writing

(2.29) $P(x, y, z) = e^{ikx} \cos s\pi z \, F(y)$,

the equations become

(2.30) $F''(y) - (k^2 + (\Delta\pi B)^2) F(y) = 0$ with

(2.31) $\delta F'(y) + k F(y) = 0$ at $y = 0, 1$.

We now solve (2.30) and (2.31) for two cases: k real and k imaginary. Real k implies wave motion along the x-coordinate while imaginary k denotes exponential behavior in x .

CASE 1 -- Real k

The only solution to 2.31 is

(2.32) $F(y) = e^{-\frac{k}{\delta} y}$, which satisfies 2.31 at all y and not just at the end points, i.e., $V \equiv 0$. The dimensional pressure is then

(2.33) $P(x, y, z, t) = Re \left\{ C_\Delta e^{i(k_\Delta x - \sigma t)} e^{-\frac{k_\Delta f}{\delta} y} \cos \frac{\Delta\pi z}{H} \right\}$.

The arbitrary constant C_Δ has dimensions $\frac{cm^2}{Sec^2}$ as P is pressure divided by density.

Using 2.18 - 2.20 we obtain for the velocity:

(2.34) $u = Re \left\{ k_\Delta C_\Delta e^{i(k_\Delta x - \sigma t)} e^{-\frac{k_\Delta f}{\delta} y} \cos \frac{\Delta\pi z}{H} \right\}$

(2.35) $V \equiv 0$

(2.36) $W = Re\left\{ -C_n \frac{n\pi}{H} \frac{i\sigma}{N^2 - \sigma^2} e^{i(k_n x - \sigma t)} e^{-\frac{k_n f}{\sigma} y} \sin \frac{n\pi z}{H} \right\}$.

The dispersion relation is obtained from the governing equation 2.30:

(2.37) $\left(\frac{k_n}{\delta}\right)^2 - \left(k_n^2 + (n\pi B)^2 \right) = 0$, and in

dimensional form this is

(2.38) $\sigma^2 = \frac{k_n^2 N^2}{k_n^2 + \left(\frac{n\pi}{H}\right)^2}$.

The solutions 2.33 - 2.38 identify the motion as a baroclinic set ($n = 1, 2, 3, \ldots$) of internal Kelvin waves. The phase speed is

(2.39) $C_p \equiv \frac{\sigma}{k} = \pm \frac{N}{\left[k^2 + \left(\frac{n\pi}{H}\right)^2\right]^{1/2}}$. Differentiating (2.38) with

respect to k we obtain

(2.40) $\frac{\sigma}{k} \frac{\partial \sigma}{\partial k} = \frac{\left(\frac{n\pi}{H}\right)^2 N^2}{\left[k^2 + \left(\frac{n\pi}{H}\right)^2\right]^2}$.

The right hand side of 2.40 is always positive, which means that the phase speed (C_p) and the group velocity ($C_g \equiv \frac{\partial \sigma}{\partial k}$) always have the same sign. Energy propagates at the group velocity, hence the phase and energy of the waves move in the same long-channel (x) direction. We are considering motion only in the negative x portion of the channel and therefore

demand that energy be allowed to propagate only in the $-x$ direction (away from the forcing at $x = 0$). We therefore restrict c_g (and hence c_p) to have negative sign. Under this constraint, the dispersion relation is

$$(2.41)\quad \sigma = \frac{-kN}{\left[k^2 + \left(\frac{2\pi}{H}\right)^2\right]^{1/2}} \quad .$$

$\frac{\sigma}{N}$ vs. k is plotted in Figure 2 for several values of $\frac{2\pi}{H}$. We note that $|\sigma| < N$, and that for a given frequency, an increase in vertical scale (H) is accompanied by an increase in horizontal wavelength ($O(\frac{1}{k})$). The figure also confirms that the phase speed and group speed are negative.

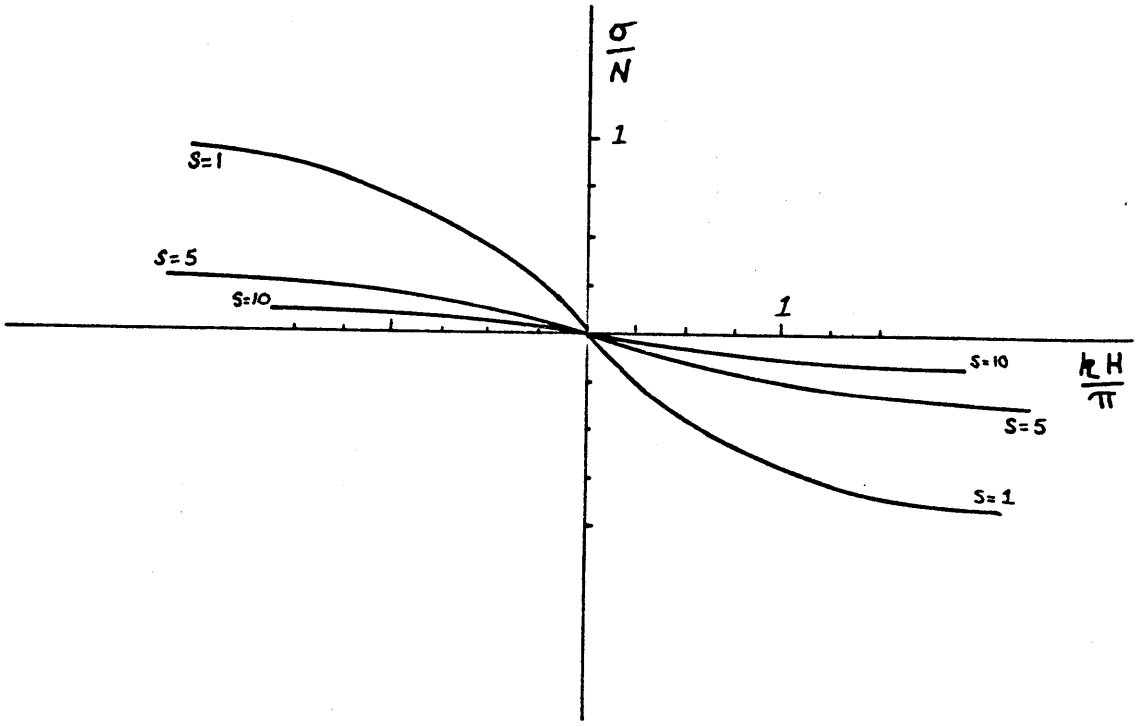

Figure 2.

Kelvin wave dispersion relation for the first, fifth and tenth vertical modes.

It is instructive to consider constant frequency curves in wave number (k, $\frac{4\pi}{H}$) space. Figure 3 is such a plot where kL and mH are the non-dimensional horizontal (χ) and vertical (z) wave numbers, respectively. In the channel, the top and bottom boundaries fix mH to values π, 2π, 3π, ..., and this effect is illustrated by the dashed horizontal lines in the figure.

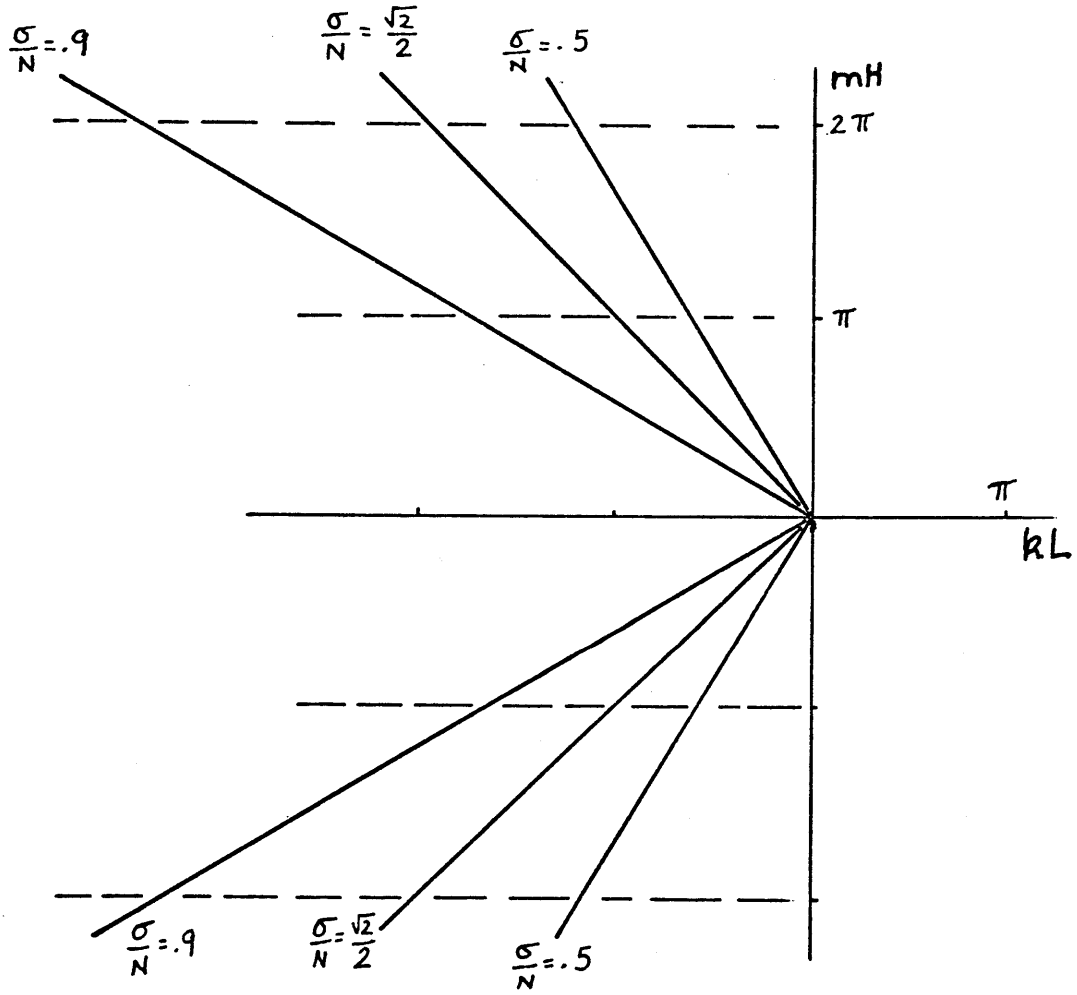

Figure 3.

Constant frequency curves in wave number space for Kelvin waves.

We see that for a given frequency ($\sigma < N$), two waves of equal horizontal wave number exist simultaneously. The vertical wave numbers ($\pm \ell \pi$) of the two have opposite sign, and the two waves combine to form standing motion in the vertical.

The cross-channel structure of the Kelvin wave is $e^{-\frac{kf}{\sigma} y}$ indicating that the waves decay exponentially away from one sidewall. The phase speed $\frac{\sigma}{k}$ is negative hence the trapping is against the $y = L$ sidewall. The motion is trapped by rotation but otherwise unaffected by it. (Note the absence of f in σ, C_p, C_g.) A rough sketch of the Kelvin wave is shown in Figure 4.

The cross-channel e-folding decay length is given by $\frac{\sigma}{kf}$.

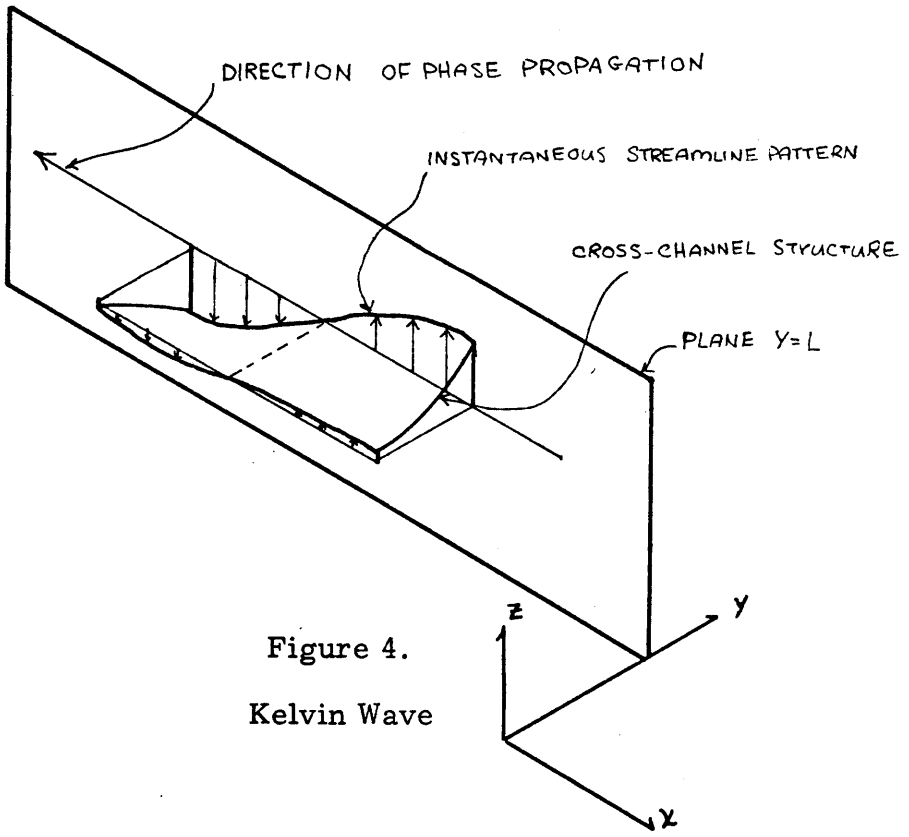

Figure 4.

Kelvin Wave

CASE 2 -- Imaginary k

If we let $k = -i\gamma$, then the behavior of the motion is exponential in x, and equations 2.30 and 2.31 become

(2.42) $$F''(y) + [\gamma^2 - (\Delta\pi B)^2] F(y) = 0$$, with

(2.43) $$\delta F'(y) - i\gamma F(y) = 0 \quad \text{at } y = 0.1 .$$

The solution is

(2.44) $$F(y) = i\gamma f \sin \ell_n y + \sigma \ell_n \cos \ell_n y$$, where

$$\ell_n = n\pi .$$

The dimensional pressure is then

(2.45) $$P(x,y,z,t) = Re \{ R_{\Delta n} e^{\gamma_{\Delta n} x} \cos \Delta\pi z [i\gamma f \sin \ell_n y + \sigma \ell_n \cos \ell_n y] e^{-i\sigma t} \} .$$

In this case, a barotropic ($\Delta = 0$) mode is allowed. Using 2.18 - 2.20, we obtain for the velocity:

(2.46) $$u = Re \{ R_{\Delta n} e^{\gamma_{\Delta n} x - i\sigma t} \cos \Delta\pi z (-i\gamma \ell_n \cos \ell_n y + \frac{\sigma f}{\sigma^2 f^2} (\gamma_{\Delta n}^2 - \ell_n^2) \sin \ell_n y) \}$$

(2.47) $$V = Re\{R_{sn} e^{\gamma_{sn}x - i\sigma t} \cos s\pi z \, (i[\gamma_{sn}^2 - l_n^2] \sin l_n y)\}$$

(2.48) $$W = Re\left\{\frac{\sigma}{N^2-\sigma^2} R_{sn} e^{\gamma_{sn}x - i\sigma t} \cos s\pi z \, (-\gamma_{sn} f \sin l_n y + i\sigma l_n \cos l_n y)\right\}$$

The solution represents standing oscillations whose amplitudes decay ($in\ x$) away from the point of forcing. In the context of our wavemaker problem, we must have $\gamma_{sn} > 0$ to insure that the amplitudes decay away from the wavemaker. The frequency and wave numbers are related by using 2.42.

(2.49) $$\gamma_{sn}^2 - l_n^2 - (s\pi B)^2 = 0$$

In dimensional form, this is

(2.50) $$\sigma^2 = \frac{(l_n^2 - \gamma_{sn}^2)N^2 + (\frac{s\pi}{H})^2 f^2}{(l_n^2 - \gamma_{sn}^2) + (\frac{s\pi}{H})^2}$$

In the low frequency limit ($\sigma << f$, $\sigma << N$), 2.50 becomes

(2.51) $$\gamma_{sn}^2 \simeq (\frac{n\pi}{L})^2 + (\frac{s\pi}{H})^2 (\frac{f}{N})^2$$, and the e-folding

decay length (x-coordinate) is given by

(2.52) $$\lambda_{e_{sn}} \equiv \frac{1}{\gamma_{sn}} = \left[(\frac{n\pi}{L})^2 + (\frac{s\pi}{H})^2 (\frac{f}{N})^2 \right]^{-1/2}.$$

which may be rewritten as

$$(2.53)\quad \frac{\lambda_e}{L_n} = \left[(n\pi)^2 + (A\pi)^2 \left(\frac{fL}{HN}\right)^2 \right]^{-1/2} .$$

$\frac{\lambda_e}{L_n}$ vs. $\frac{fL}{HN}$ for several horizontal (n) and vertical (A) modes is plotted in Figure 5.

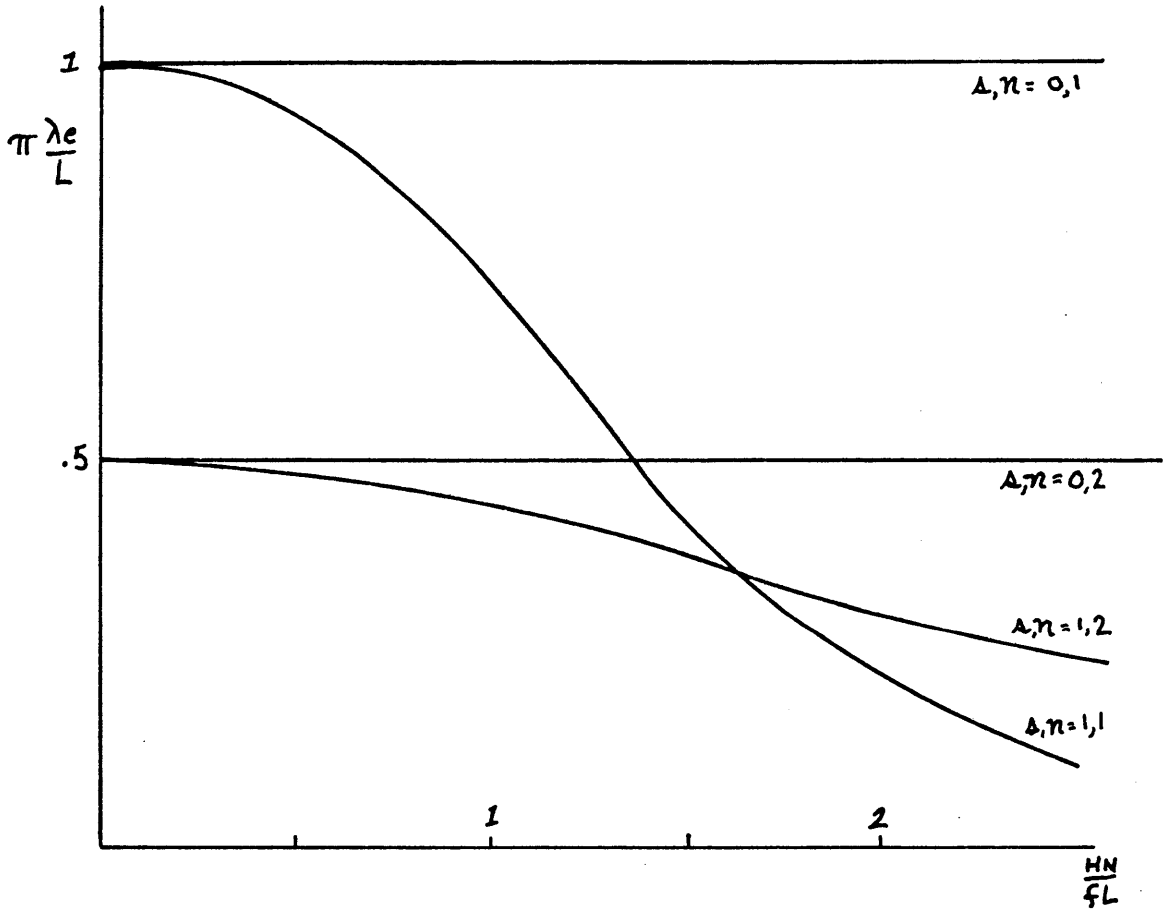

Figure 5.

Decay of Standing Waves

We see in the figure that the least trapped mode for any $\frac{fL}{NH}$ is the first cross-channel ($n=1$), barotropic ($\ell=0$) mode (with $\lambda_{01}^{e} = \frac{L}{\pi}$), and that the trapping increases with increasing $\frac{fL}{NH}$.

The standing oscillations provide continuity between the fluid and the wavemaker, and as we shall see later in this chapter, they are incapable of transporting energy across planes x constant.

Now that we have examined the modes in a flat bottom channel, let us return to equations 2.24 - 2.27 and solve for the case of small slope, $\epsilon << 1$.

We can transform the bottom boundary condition to hold on a constant surface by means of a coordinate transformation introduced by Phillips (1957). We define a new coordinate system, (x, y, η), where $\eta = \frac{z - \epsilon y}{1 - \epsilon y}$. The surface $z = \epsilon y$ becomes the constant surface $\eta = 0$, while the surface $z = 1$ remains constant, $\eta = 1$. (See Figure 6.)

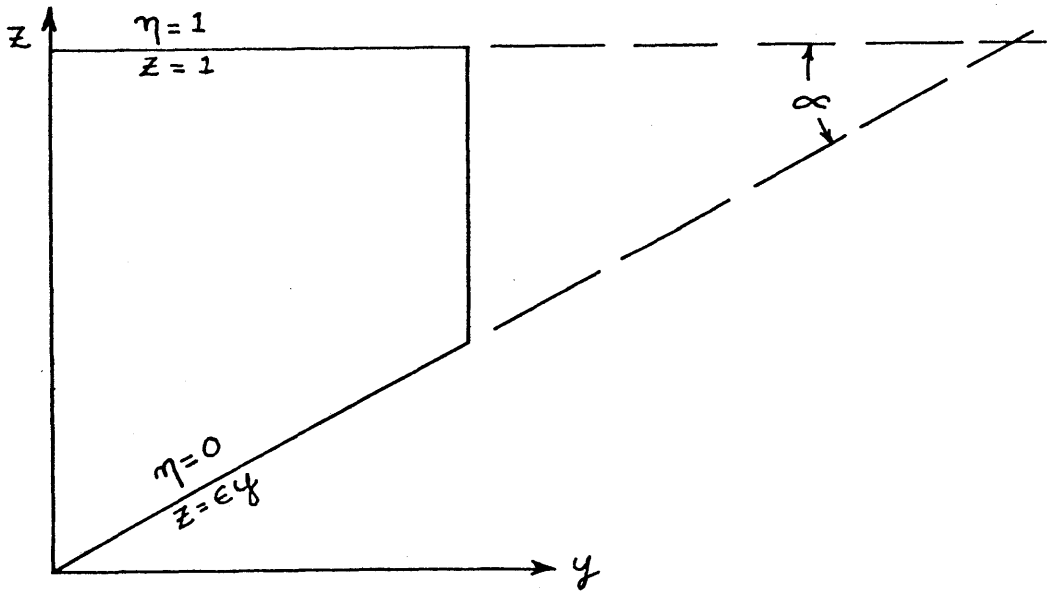

Figure 6.

Transformation of the bottom boundary to a constant surface.

We must similiarly transform equations 2.24 - 2.27. The x, y, and z derivatives transform as follows:

$$(2.54)\quad \left(\frac{\partial}{\partial y}\right)_z = \left(\frac{\partial}{\partial y}\right)_\eta + \epsilon \frac{(\eta-1)}{1-\epsilon y}\left(\frac{\partial}{\partial \eta}\right)_y \quad ,$$

$$(2.55)\quad \left(\frac{\partial}{\partial z}\right)_y = \left(\frac{1}{1-\epsilon y}\right)\left(\frac{\partial}{\partial \eta}\right)_y \quad ,$$

$$(2.56)\quad \left(\frac{\partial^2}{\partial y^2}\right)_z = \left(\frac{\partial^2}{\partial y^2}\right)_\eta + \frac{2\epsilon(\eta-1)}{1-\epsilon y}\frac{\partial^2}{\partial \eta \partial y} + \frac{2\epsilon^2(\eta-1)}{(1-\epsilon y)^2}\frac{\partial}{\partial \eta} + \left[\frac{\epsilon(\eta-1)}{1-\epsilon y}\right]^2 \frac{\partial^2}{\partial \eta^2} \quad ,$$

$$(2.57)\quad \left(\frac{\partial^2}{\partial z^2}\right)_y = \left(\frac{1}{1-\epsilon y}\right)^2 \left(\frac{\partial^2}{\partial \eta^2}\right)_y .$$

In the new system, the equations become:

$$(2.58)\quad P_{xx} + P_{yy} + 2(\eta-1)(\epsilon+\epsilon^2 y+\cdots)P_{\eta y} + 2(\eta-1)(\epsilon^2+2\epsilon^3 y+\cdots)P_\eta + (\eta-1)^2(\epsilon^2+2\epsilon^3 y+\cdots)P_{\eta\eta} + B^2(1+2\epsilon y+\cdots)P_{\eta\eta} = 0$$

$$(2.59)\quad P_\eta(1+\epsilon y+\cdots) = 0 \quad \text{at } \eta = 1,$$

$$(2.60)\quad P_x + i\delta\{P_y + (\eta-1)(\epsilon+\epsilon^2 y+\cdots)P_\eta\} = 0 \quad \text{at } y = 0, 1 .$$

(2.61) $i\delta B^2(1+\epsilon y+\cdots)P_\eta = \epsilon\{P_x + i\delta[P_y + (\eta-1)(\epsilon+\epsilon^2 y+\cdots)P_\eta]\}$ at $\eta=0$.

We now expand P in powers of ϵ: $P = P^{(0)} + \epsilon P^{(1)} + \epsilon^2 P^{(2)} + \ldots$, and separate out the x-dependence by writing $P(x,y,z) = G(y,z)e^{ikx}$. We will solve two cases: Case 1 in which $O(k) = O(\epsilon)$, $O(\epsilon) = O(\delta)$ and Case 2 in which $O(k) = O(1)$, $O(\epsilon) = O(\delta)$. We assume that $\epsilon \ll 1$ throughout the following analysis in order that the perturbation expansion be valid.

CASE 1 $\quad O(\epsilon) = O(\delta), \quad O(k) = O(\epsilon)$

The ϵ^0 governing equation is

(2.62) $G^{(0)}_{yy} + B^2 G^{(0)}_{\eta\eta} = 0$, with the boundary conditions:

(2.63) $G^{(0)}_\eta = 0$ at $\eta = 0, 1$,

(2.64) $kG^{(0)} + \delta G^{(0)}_y = 0$ at $y = 0, 1$.

This is essentially the same set of equations solved for Case 1 of the flat-bottom channel analysis. The solution is (dropping superscripts)

(2.65) $G(y,z) = e^{-\frac{k}{\delta}y}\cos s\pi\eta$, yielding for the lowest order pressure:

(2.68) $P(x,y,\eta,t) = Re\{D_s e^{i(k_s x - \sigma t)} e^{-\frac{k_s f}{\delta}y}\cos\frac{s\pi\eta}{H}$.

These baroclinic Kelvin waves persist (to lowest order) when the bottom is sloped because the particle motion accompanying Kelvin waves is along contours of constant fluid height ($V \equiv 0$).

CASE 2 $\quad O(\epsilon) = O(\delta),\ O(k) = O(1)$

The ϵ^0 governing equation is

(2.67) $G^{(0)}_{yy} + B^2 G^{(0)}_{\eta\eta} - k^2 G^{(0)} = 0$, with the

boundary conditions

(2.68) $G^{(0)} = 0$ at $y = 0, 1$,

(2.69) $G^{(0)}_{\eta} = 0$ at $\eta = 1$, and

(2.70) $\delta B^2 G^{(0)}_{\eta} = \epsilon k G^{(0)}$ at $\eta = 0$.

B is now $\cong \frac{f}{N}$ since $\sigma \ll f$, $\sigma \ll N$. The boundary conditions (2.68) require that the y -dependence by $\sin n\pi y$.

Let $\ell_n = n\pi$ and write $G^{(0)} = \sin \ell_n y \, F(\eta)$. The set of equations 2.67 - 2.70 then becomes

(2.71) $$F''(\eta) - \frac{(k_n^2 + \ell_n^2)}{B} F(\eta) = 0$$, with the

boundary conditions

(2.72) $$F'(\eta) = 0$$ at $\eta = 1$, and

(2.73) $$\delta B^2 F'(\eta) = \epsilon k F(\eta)$$ at $\eta = 0$.

The solution to 2.71 and 2.72 is

(2.74) $$F(\eta) = \cosh \mu_n (\eta - 1)$$, where $\mu_n = \frac{(k_n^2 + \ell_n^2)^{1/2}}{B}$,

yielding for the pressure

(2.75) $$P^{(0)}(x, y, \eta, t) = Re\{\alpha_n e^{i(k_n x - \sigma t)} \sin \ell_n y \cosh \mu_n (\eta - 1)\}.$$

This solution was studied in detail by Rhines (1970). The motion arises due to the sloping bottom, and will be referred to as a topographic wave.

The dispersion relation is obtained from the bottom boundary condition, and is

$$(2.76)\quad \delta = -\frac{\epsilon k_n}{B^2 \mu_n} \coth \mu_n .$$

Dimensionally, this is

$$(2.77)\quad \sigma = -\frac{SN^2 k_n}{f \mu_n} \coth \mu_n H \quad , \text{ where } k_n \text{ and } \mu_n$$

are now dimensional quantities. Replacing μ_n in 2.77 by $\frac{(k_n^2 + \ell_n^2)^{1/2}}{B} = \frac{N}{f}(k_n^2 + \ell_n^2)^{1/2} \equiv \frac{KN}{f}$, we have

$$(2.78)\quad \sigma = -\frac{SNk_n}{K_n} \coth \frac{K_n HN}{f} .$$

The dispersion relation will be discussed in detail, but let us first examine the vertical structure of the topographic motion.

In the low frequency limit, $u \sim P_y$ and $V \sim P_x$. Thus the horizontal velocity components have the vertical structure $\cosh \frac{K_n HN}{f}(\eta - 1)$. (η is non-dimensionalized by H). The vertical structure of the horizontal velocity amplitude is plotted in Figure 7 for several values of $\frac{KHN}{f}$.

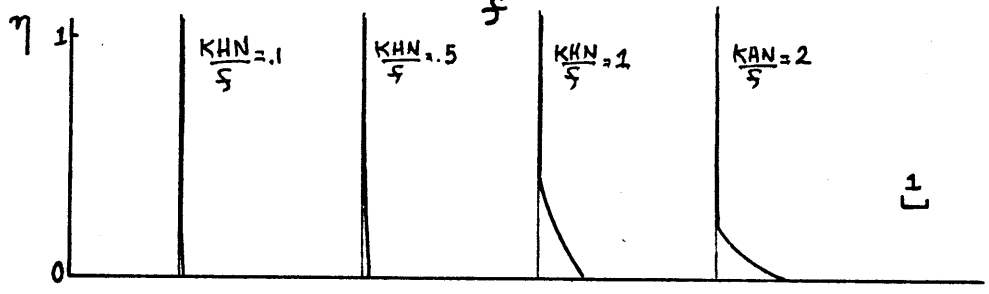

Figure 7.

Vertical structure of the topographic wave.

We see that the motion is strongly trapped to the bottom when $\frac{KHN}{f} \gtrsim 1$, but is essentially barotropic when $\frac{KHN}{f} \ll 1$. The vertical e-folding decay length of the trapped waves is $O(\frac{f}{KN})$. We will now see that when $\frac{KHN}{f}$ is small, the motion resembles that of topographic Rossby waves.

In the limit of small $\frac{KHN}{f}$, $Tanh \frac{KHN}{f} \sim \frac{KHN}{f}$, and the dispersion relation (2.78) becomes

$$(2.79)\quad \sigma = -\frac{SN k_n}{K_n}\left(\frac{1}{\frac{K_n H N}{f}}\right) = -\frac{\epsilon f}{L}\left(\frac{k_n}{k_n^2 + l_n^2}\right),$$

which is the formula for topographic Rossby waves. Note the absence of N in the dispersion relation, indicating that the motion is not a buoyancy oscillation. This is expected because the motion is essentially barotropic when $\frac{KHN}{f} \ll 1$.

The phase speed,

$$(2.80)\quad \frac{\sigma}{k_n} = \frac{-\epsilon f}{L}\left(\frac{1}{k_n^2 + l_n^2}\right)$$

, has the opposite sign of ϵ.

This means that if $\epsilon > 0$ (shallow water to the north, or $+y$ direction) there is always a component of phase propagation to the west (or $-x$ direction). The down-channel group velocity,

$$(2.81)\quad \frac{\partial \sigma}{\partial k} = \frac{\epsilon f}{L}\frac{k^2 - l^2}{(k^2 + l^2)^2}$$

, is bi-directional, depending on the

relative sizes of k and ℓ. These results are summarized by the plot of constant frequency curves in wave number space (Figure 8). The wave numbers are non-dimensionalized by L, and the effect of the sidewalls in fixing ℓ_n to values $n\pi$ is indicated by the horizontal dashed lines.

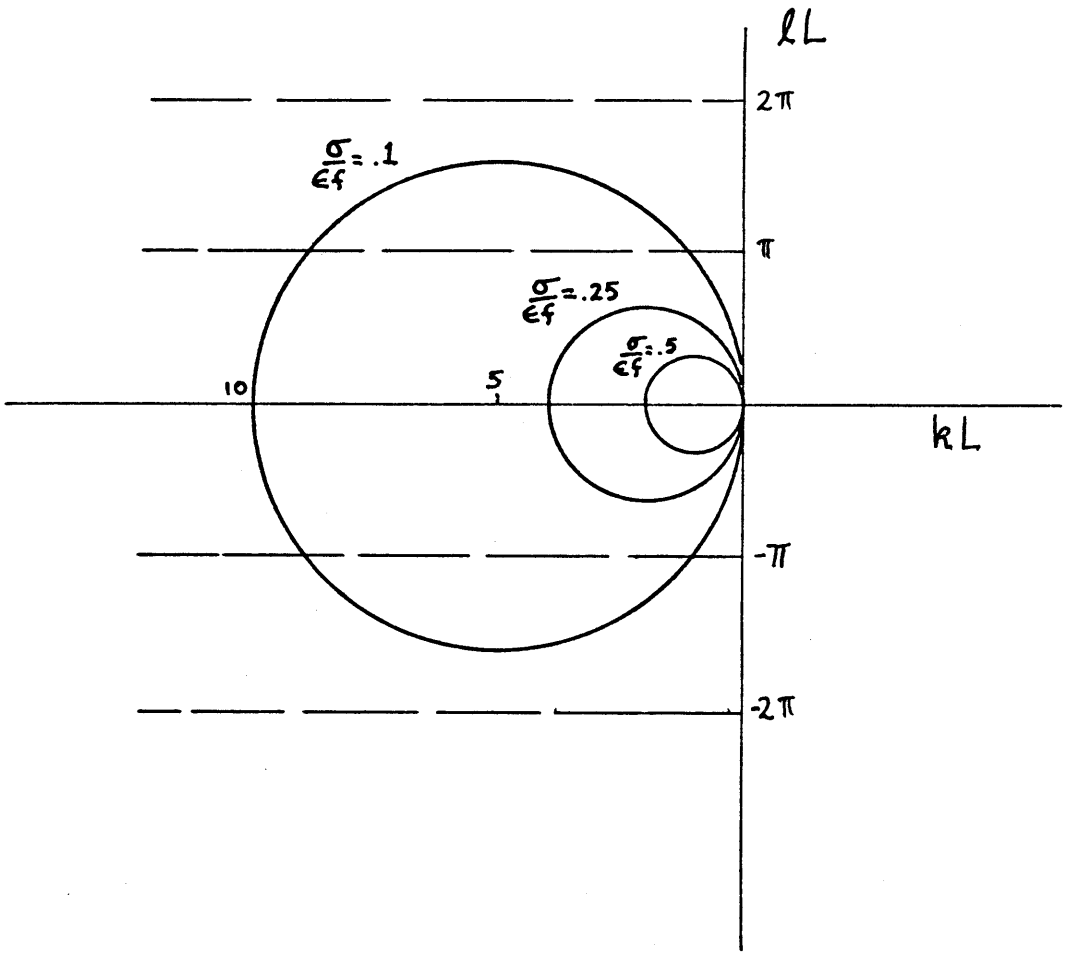

Figure 8.

Constant frequency curves in wave number space for topographic Rossby waves.

We see in the figure that the down-channel group velocity, $\frac{\partial \sigma}{\partial k}$, changes sign where $k^2 = \ell^2$. If $\frac{\sigma}{\epsilon f}$ is fixed, the presence of vertical walls allows two sets of incident and reflected pairs of waves -- one set lying to the left of the lines $k^2 = \ell^2$, and the other set lying to the right (see Figure 9).

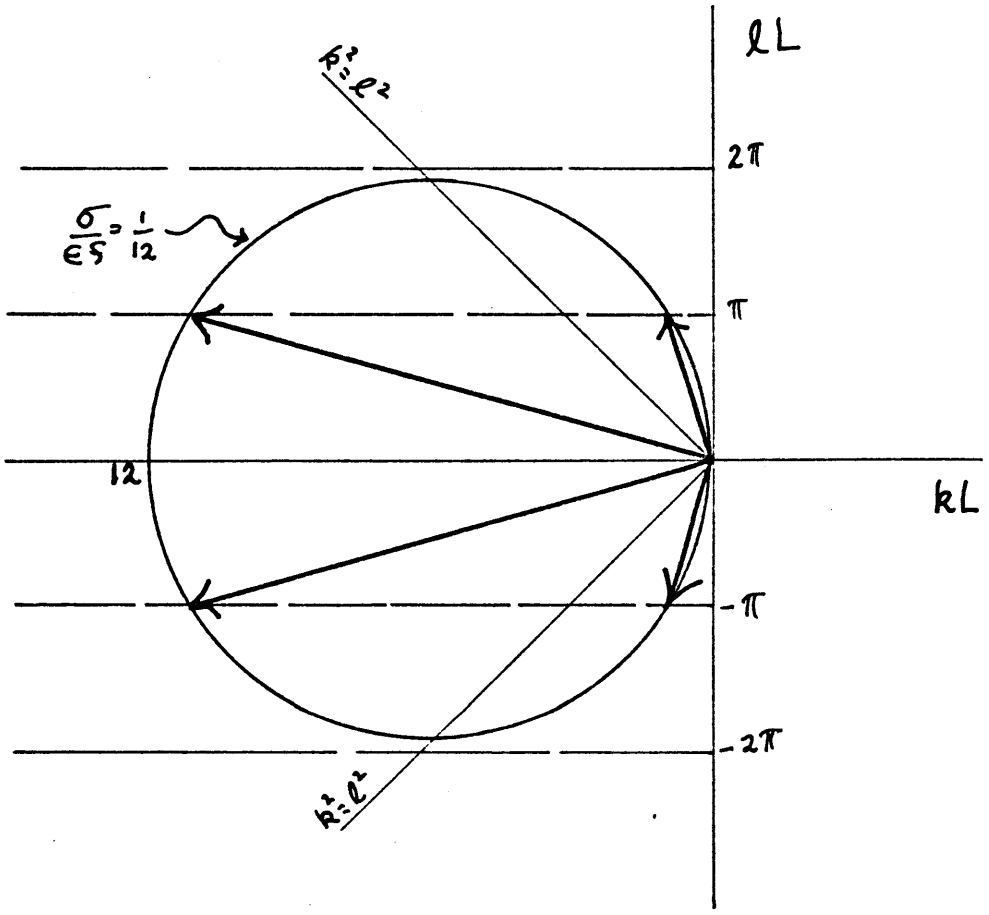

Figure 9.

Diagram of the waves allowed for fixed ℓ at a given value of $\frac{\sigma}{\epsilon f}$.

The left pair has down-channel group velocity to the East ($+\chi$) and the right pair has westward group velocity. Each pair consists of an incident and reflected wave, and the two add to produce standing motion along the y coordinate. The net result is two propagating waves of different wave length. The two have the same direction of phase propagation, but the opposite direction of energy propagation.

Having investigated the topographic wave behavior when $\frac{KHN}{f} \ll 1$, let us now examine the case $\frac{KHN}{f} \gtrsim 1$. We have already seen that these waves are trapped to the bottom and will henceforth refer to them as bottom-trapped waves.

As $\frac{KHN}{f}$ becomes greater than 1, $Tanh \frac{KHN}{f}$ rapidly approaches 1, and the dispersion relation (2.78) becomes

$$(2.82) \quad \sigma = \frac{-SNK_n}{K_n} = \frac{-SNk}{(k^2+l^2)^{1/2}}.$$

The phase speed, $\frac{\sigma}{k}$, has the opposite sign of S (the phase moves to the left of an observer who is facing shallow water) as does the χ-component of group velocity, $\frac{\partial \sigma}{\partial k} = -SNl^2(k^2+l^2)^{-3/2}$. Therefore, both the phase and energy of the bottom-trapped waves move to the west. These results are summarized in Figure 10, which is a plot of constant $\frac{\sigma}{SN}$ curves in wave number space. The effect of vertical walls (in fixing l to the values π, 2π, ...) is shown by the dashed lines.

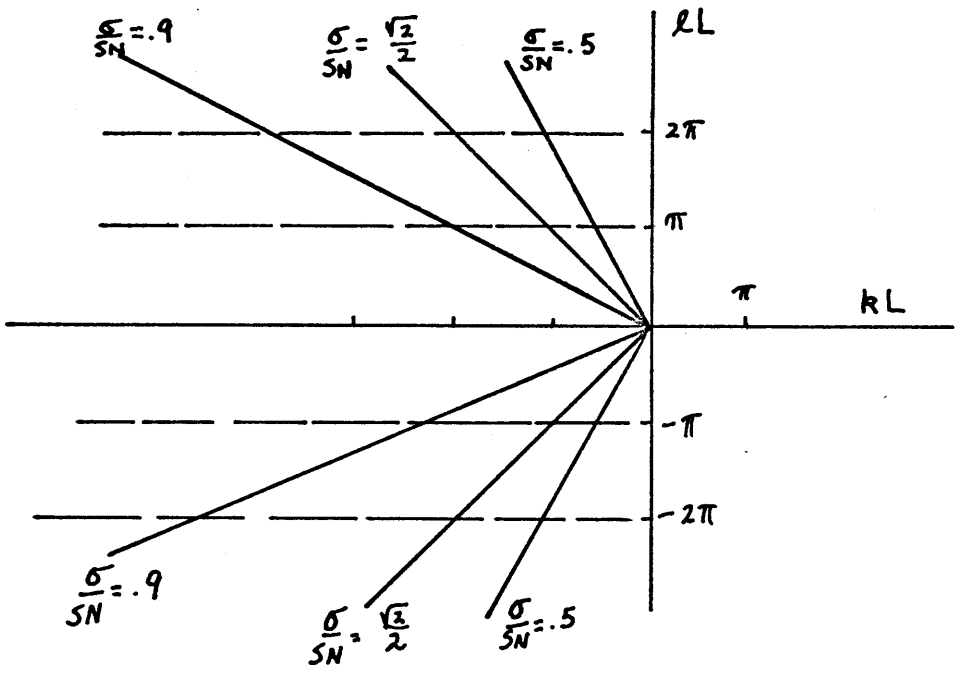

Figure 10.

Constant frequency curves in wave number space for the bottom-trapped waves. The dashed lines indicate the discrete values of ℓ allowed by the sidewalls.

We see that at a given frequency, a single incident-reflected pair of waves is excited for each cross-channel (n) mode. Each pair adds to produce a single propagating (down-channel) wave exhibiting standing motion along the cross-channel (y) axis. A rough sketch of a single mode of the bottom-trapped wave is shown in Figure 11.

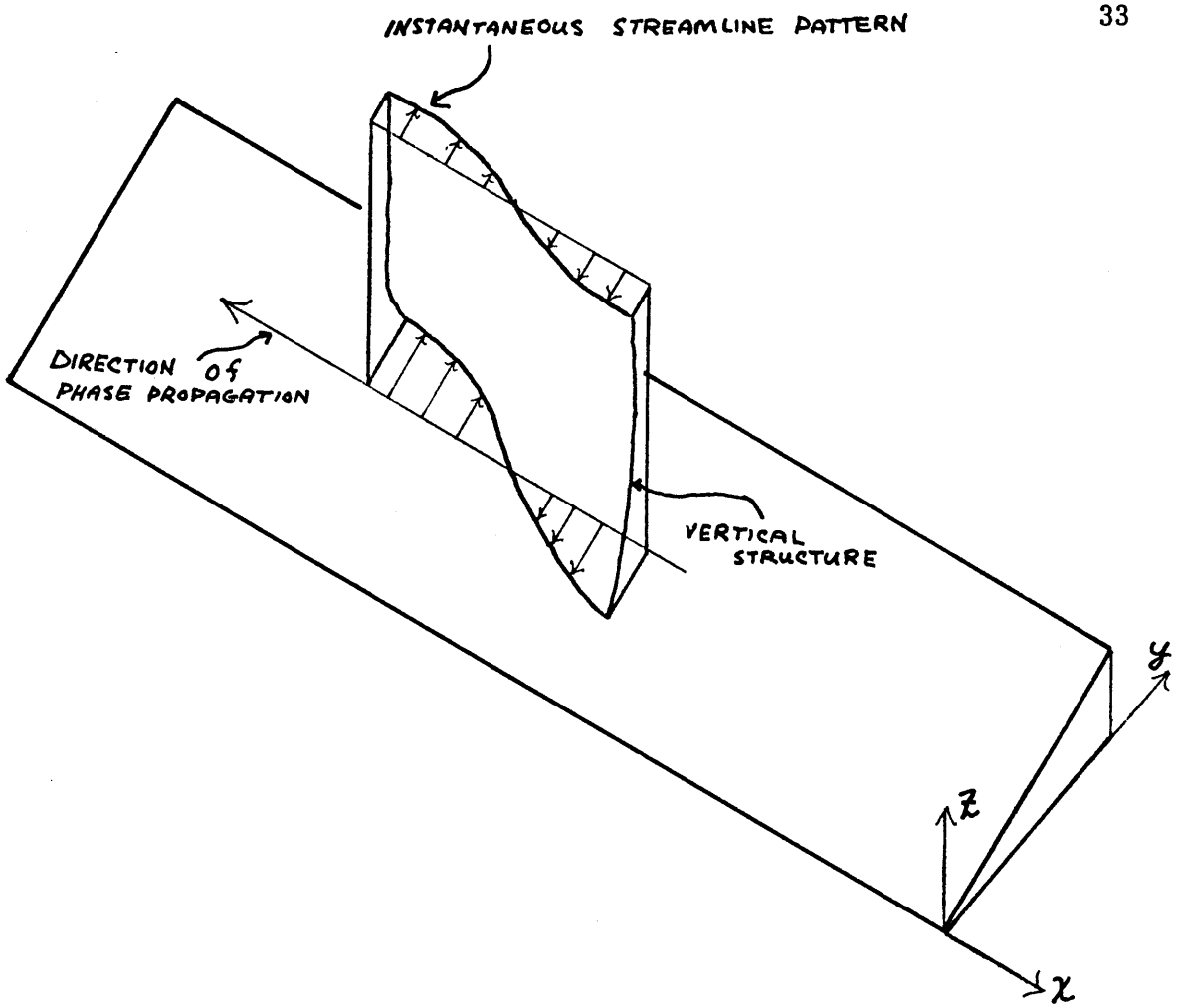

Figure 11.

The bottom-trapped wave.

Figure 10 shows that for a given wavemaker frequency ($\sigma < SN$) all of the cross-channel (n) modes will be excited. This is unlike the case of topographic Rossby waves in which only a finite number of the cross-channel modes are excited at a given frequency.

Thus far we have only looked at the limiting cases of $\frac{KHN}{f} \ll 1$ and

$\frac{KHN}{f} \gtrsim 1$, and will now solve the complete dispersion relation, $\frac{\sigma}{SN} = -\frac{k}{K} \coth \frac{KHN}{f}$. If we scale k and ℓ by L , the dispersion relation may be written:

$$(2.83)\quad \frac{\sigma}{SN} = \frac{-k}{(k^2+\ell^2)^{1/2}} \coth (k^2+\ell^2)^{1/2} \frac{HN}{fL} \quad , \text{ where}$$

k and ℓ are non-dimensional. Solutions (k, ℓ) to 2.83 were computed for several values of $\frac{HN}{fL}$ and $\frac{\sigma}{SN}$, and the results are sketched (as constant $\frac{\sigma}{SN}$ curves in wave number space) in Figure 12. We see that when $\sigma \gtrsim SN$, the curves of constant $\frac{\sigma}{SN}$ form closed semi-elliptical curves in the wave number space, looking much like the curves in the topographic Rossby wave limit. The curves have a mean radius of $\simeq \frac{1}{2}\left(\frac{\sigma}{SN}\right)^{-1}\left(\frac{HN}{fL}\right)^{-1} = \frac{\epsilon f}{2\sigma}$ and when $\sigma < SN$, the curves are no longer closed, but resemble parabolas which rapidly become linear away from the origin. These parabolas belong to the bottom-trapped regime of topographic waves in which a single wave is excited with a given ℓ-wave number. The dashed horizontal lines again show the effect of the sidewalls in quantizing ℓ .

For fixed frequency, we see that the sidewalls have the effect of restricting the number of topographic waves excited to a finite number. In fact, if $\frac{HN}{fL}$ is greater than $\sim .22$, none of the topographic Rossby waves will be excited for any frequency. This is easily seen in Figure 13, which shows constant frequency curves plotted in wave number space scaled by $\frac{HN}{fL}$. This plot places the $\frac{HN}{fL}$ dependence on the axes and therefore summarizes the plot in Figure 12. At the "topographic Rossby

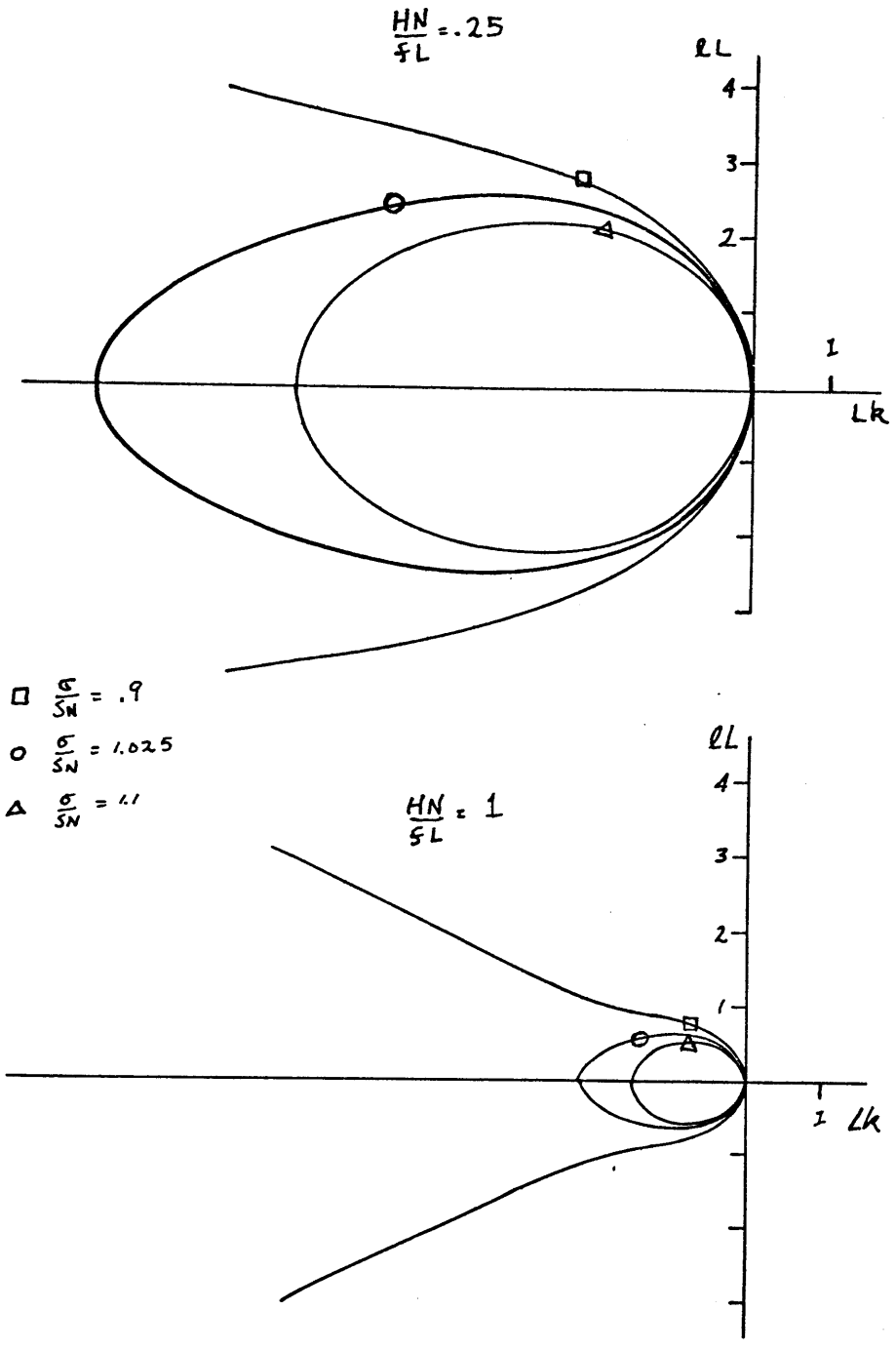

Figure 12.

Constant frequency curves for topographic waves. k and ℓ are non-dimensional wave numbers.

wave cut-off" frequency of $\sigma = sN$, the topographic Rossby wave curve reaches its maximum ordinate value of $\sim .69$. The largest value of ℓ is then $\ell = .69\left(\frac{HN}{fL}\right)^{-1}$, while the smallest ℓ allowed by the vertical walls is π ($n=1$ mode). Hence $\frac{HN}{fL}$ must be smaller than $\frac{.69}{\pi}$ if even one topographic Rossby wave mode is to be excited.

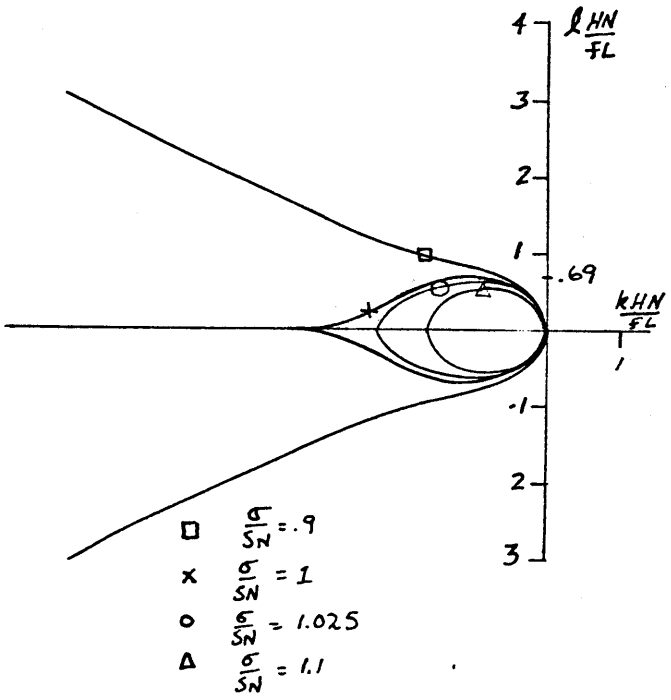

Figure 13.

Constant frequency curves for topographic waves. $\frac{k}{L}$ and $\frac{\ell}{L}$ are dimensional wave numbers.

If we are to see even the first topographic Rossby wave mode in the channel, we must insure that (i) $\sigma \geq sN$ and (ii) $\frac{HN}{fL} \leq .22$. On the other hand, all of the bottom-trapped wave modes exist as long as the excitation (wavemaker) frequency is less than sN. The bottom-trapped waves are thus easily isolated in the channel and a laboratory experiment to study their behavior can easily be designed to eliminate the topographic Rossby waves.

If the wavemaker frequency is less than sN we have the bottom-trapped topographic waves and the Kelvin waves to match to the wavemaker at $\chi = 0$. As will be seen in more detail, a wavemaker whose motion is symmetric in y , i.e., $\int_0^L u_{WM}\, dy = 0$, cannot excite Kelvin waves.

Assuming that we have such a wavemaker, we are left with only the bottom-trapped waves. A problem now arises because the set of bottom-trapped modes is not complete. There are an infinite number of wavemaker vertical profiles (of χ-velocity) which the set $\{\cosh \mu_n(\eta-1)\}$ cannot completely describe. In the matching problem, we decompose the χ-velocity of each bottom-trapped wave mode as well as the χ-velocity of the wavemaker into complete orthogonal sets $\{a_0,\ a_\beta \cos \beta\pi\eta\}$, and then equate coefficients of the cosine functions. The following is a rough outline of the matching problem -- the details will be given in Chapter 3.

Considering only the vertical structure of the wavemaker, we expand the χ-component of the wavemaker velocity in the complete set $\{A_0 + A_\beta \cos \beta\pi\eta\}$, i.e.,

(2.84) $$u_{WM} = A_0 + \sum_\beta A_\beta \cos \beta\pi\eta \quad .$$

We similiarly expand all of the bottom-trapped modes:

$$(2.85)\quad \begin{aligned} u_{BT} &= \sum_n \alpha_n \cosh \mu_n (\eta - 1) \\ &= \sum_n \alpha_n \left(a_{0n} + \sum_s a_{sn} \cos s\pi\eta \right) \end{aligned} .$$

Equating coefficients of the cosine terms in 2.84 and 2.85, we find that

$$(2.86)\quad \sum_n \alpha_n a_{0n} = A_0 \quad , \text{ and}$$

$$(2.87)\quad \sum_n \alpha_n a_{sn} = A_s \quad .$$

Writing 2.86 and 2.87 in matrix notation, we have

$$(2.88)\quad \begin{bmatrix} A_0 \\ A_1 \\ A_2 \\ \vdots \end{bmatrix} = \begin{bmatrix} a_{01} & a_{02} & a_{03} \cdots \\ a_{11} & a_{12} & a_{13} \cdots \\ a_{21} & a_{22} & a_{23} \cdots \\ \vdots & \vdots & \vdots \end{bmatrix} \begin{bmatrix} \alpha_1 \\ \alpha_2 \\ \alpha_3 \\ \vdots \end{bmatrix} ,$$

which must be solved for the unknowns $\alpha_1, \alpha_2, \ldots$. In practice, we truncate the matrix at an equal number of rows and columns, and then form the inversion matrix to find α_n. The success of this method depends on whether or not the values obtained for α_n converge to a fixed number as more and more elements of the matching matrix are retained. The values do not converge in general, as illustrated by the following example.

Suppose the wavemaker excursion is zero in the bottom half of the channel and finite in the top half. Bottom-trapped waves cannot be excited since no energy is supplied to their "region of motion". We must have more modes (other than bottom-trapped) if we are to match the fluid to a general wavemaker. The problem is resolved by reconsidering the case of the flat-bottom channel. Recall that we found standing modes trapped near the wavemaker which provided continuity between the wavemaker and the fluid. We will show that these standing modes still exist when ϵ is increased above zero.

Recall the topographic dispersion relation ($\epsilon > 0$, Case 2):

$$(2.89)\quad \frac{\sigma}{SN}\,\mathrm{Tanh}\,\frac{KHN}{f} = -\frac{k}{K} \quad .$$

We previously considered only real solutions k and ℓ to this equation, and will now see that there are also complex k solutions which become the x-decaying standing oscillations of the flat-bottom case when $\epsilon \to 0$. Before we find the complex solutions, however, let us examine the structure of the corresponding wave.

The pressure of the topographic wave for complex k, μ, and ℓ is

$$(2.90)\quad P \sim e^{i(c+id)x - i\sigma t}\,\mathrm{Sin}(\ell+ir)y\,\mathrm{Cosh}(a+ib)(\eta-1)$$

where $k = c+id$, $\ell = \ell+ir$, and $\mu = a+ib$.

The cross-channel boundary conditions require that $Sin(\ell+ir)=0$ at $y=0,L$. This implies that $\ell+ir=\frac{n\pi}{L}$, a real number. Hence ℓ must be purely real. 2.90 is rewritten as

(2.91) $$P_n e^{-\alpha x} e^{i(cx-\sigma t)} Sin\, \ell y \left(e^{(a+ib)(\eta-1)} + e^{-(a+ib)(\eta-1)}\right) =$$

$$e^{-\alpha x} Sin\, \ell y \left\{ e^{a(\eta-1)} e^{i(cx+b(\eta-1)-\sigma t)} \right.$$

$$\left. + e^{-a(\eta-1)} e^{i(cx-b(\eta-1)-\sigma t)} \right\}$$

, which represents two waves with wave vectors ($c, 0, \pm b$). We insist that the amplitude decay ($-\alpha$) be positive, i.e., $\alpha<0$, so that the motion does not grow away from the wavemaker (in the negative x direction). The two phase propagating waves add to create standing motion in the vertical. Although there is phase propagation, energy cannot be carried down the channel. The motion decays away from the wavemaker (in a distance of $O(\frac{L}{\alpha})$), and the only sink for the energy is fluid friction, which is zero in our inviscid problem. We now find these complex k solutions.

Written in terms of μ_n , 2.89 becomes

(2.92) $$\frac{\sigma}{SN} Tanh\, \mu_n = -\left[1-\left(\frac{\ell_n}{\mu_n B}\right)^2\right]^{1/2},$$

where μ_n is non-dimensional (scaled by H). We find the complex μ_n solutions by solving

(2.93) $$\frac{\sigma}{SN}\left[1-\left(\frac{n\pi}{B}\right)^2 \frac{1}{(a+ib)^2}\right]^{1/2} = Tanh\,(a+ib)$$

for a and b . Separating the real and imaginary parts of 2.93, we obtain two simultaneous transcendental equations in the unknowns a and b:

$$(2.94)\quad 0 = \left(\frac{SN}{\sigma}\right)^2\left[1-\left(\frac{n\pi}{\beta}\right)^2\frac{(a^2-b^2)}{(a^2+b^2)^2}\right]-\frac{1}{4}\left[\frac{\sinh^2 2a-\sin^2 2b}{(\cos^2 b+\sinh^2 a)^2}\right],$$

$$(2.95)\quad 0 = \left(\frac{SN}{\sigma}\right)^2\left[\left(\frac{n\pi}{\beta}\right)^2\frac{ab}{(a^2+b^2)^2}\right]-\frac{1}{4}\left[\frac{\sinh 2a\,\sin 2b}{(\cos^2 b+\sinh^2 a)^2}\right].$$

The solutions (a, b) to these equations were found graphically with the aid of the M.I.T.- I.P.C. computer for the first $(n=1)$ mode, and the results are shown in Figure 14. This is a plot in (a, b) space for continuous values of $\frac{SN}{\sigma}$ ranging from zero to very large.

When $\frac{\sigma}{SN}<1$, purely real values of μ $(b=0)$ are allowed corresponding to the bottom-trapped waves. These exist simultaneously with the complex μ $(b\neq 0)$ solutions and are plotted on the a-axis in Figure 14. Note that when $\frac{SN}{\sigma}=0$ (flat-bottom) we indeed recover the standing oscillations (low frequency) obtained in the earlier flat-bottom analysis. As the value of $\frac{SN}{\sigma}$ increases from zero, the roots (a, b) migrate from the points $(0,0)$, $(0,\pi)$, $(0,2\pi)$,....., to the points $(0,\frac{\pi}{2})$, $(0,\frac{3\pi}{2})$, $(0,\frac{5\pi}{2})$,.....along curved paths.

The points $k=c+id \equiv (c, d)$ similiarly migrate from points on the imaginary axis to points slightly higher on the same axis. (See Figure 15.)

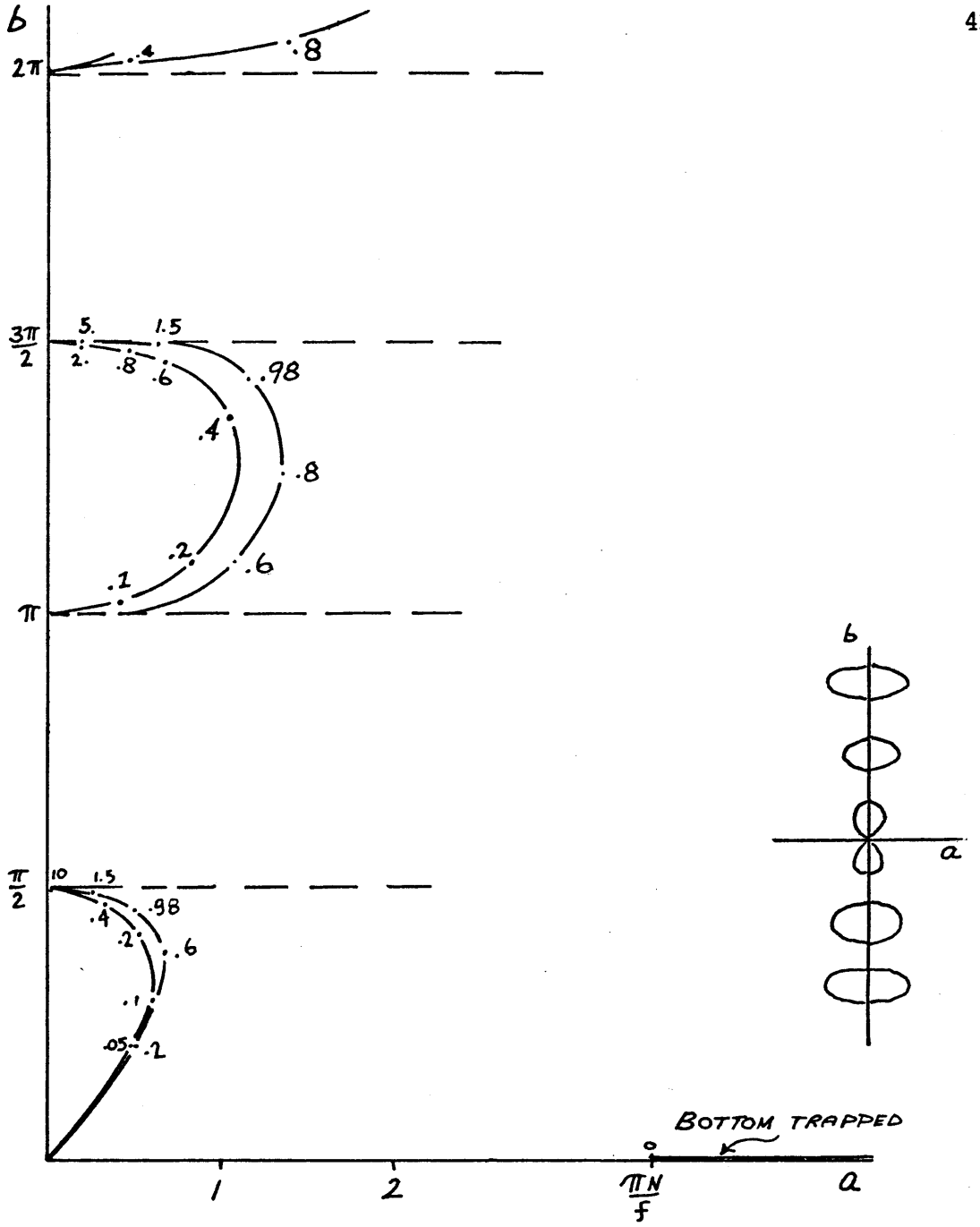

Figure 14.

Complex μ solutions to the topographic wave dispersion relation. Numbers on curves denote values of $\frac{SN}{\sigma}$. The inner curves are for $\frac{N}{f} = 4$, and the outer curves are for $\frac{N}{f} = 1.1$.

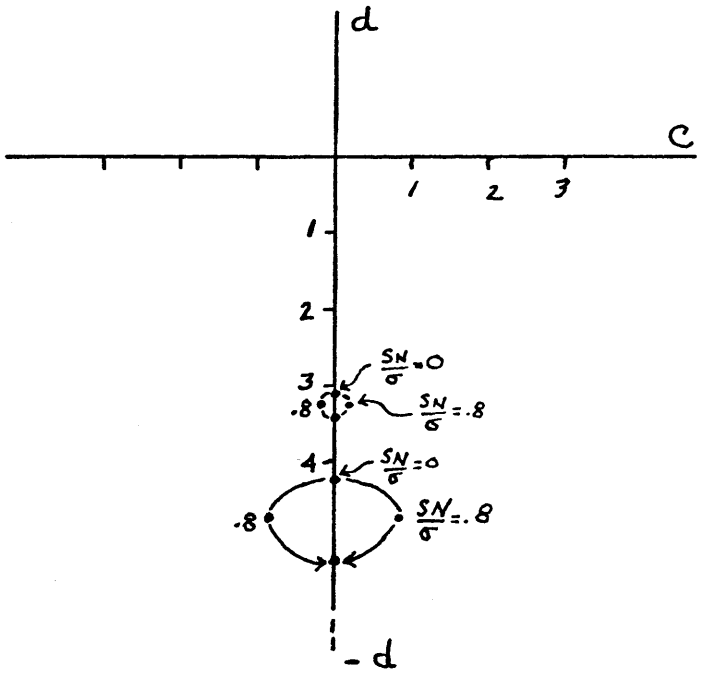

Figure 15.

Plot in (c, d) space for the complex wave number $k = c + id$.
Horizontal structure is $e^{i(kx)} = e^{-dx + icx}$.

The down-channel structure is $e^{i(kx - \sigma t)}$, so in the limits $\frac{SN}{\sigma} \to 0$ (flat-bottom) and $\frac{SN}{\sigma} >> 1$, the down-channel behavior is exponential (decay) rather than oscillatory. In the limit $\frac{SN}{\sigma} >> 1$, the vertical structure (Figure 14) becomes $\cosh(i\frac{\Delta\pi}{2}\eta) = \cos\frac{\Delta\pi}{2}\eta$ ($\Delta = 1, 3, 5, 7, \ldots$), which is zero on the bottom for all vertical (Δ) modes. This limit is interesting, because the horizontal velocities (u and v) have this structure, and hence are zero on the bottom. These modes cannot be

matched to a wavemaker having non-zero excursion at the bottom -- the bottom-trapped waves arise to fill this role. This is similiar to Suarez' (1971) analysis in which a steady geostrophic flow instantaneously comes in contact with a region with sloping bottom, i.e., $\epsilon = 0$ at $t = 0$ and $\epsilon > 0$ for $t > 0$. The response, as illustrated by Suarez, is shown in Figure 16. For $t > 0$, the steady flow has a node at the bottom, and the bottom-trapped wave arises to continue the "flow of energy" near the bottom. The initial geostrophic current may be vertically dependent -- the only part of the flow that induces bottom trapped oscillations is its value at the bottom.

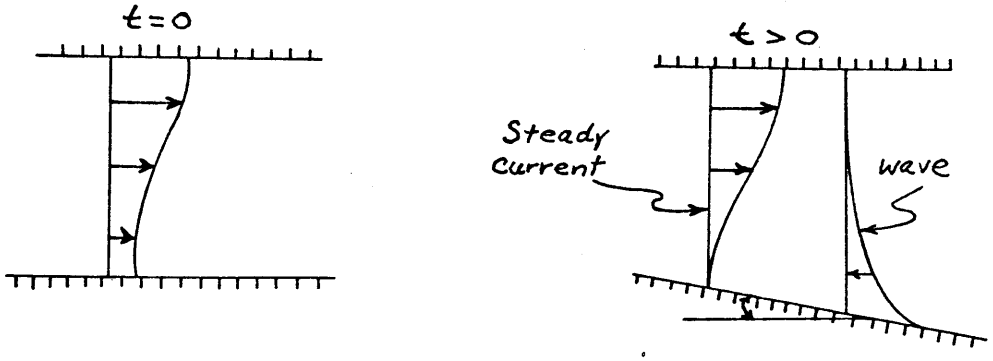

Figure 16.

Diagram illustrating the vertical structure of geostrophic currents. From Suarez (1971).

In the case of the wavemaker problem, a component of flow across constant depth contours may be induced. The standing oscillations (providing continuity between the fluid and the wavemaker) then have horizontal velocity nodes at the bottom, and the bottom-trapped wave is necessary to complete the coupling in the vertical.

We have already indicated that the Kelvin and bottom-trapped waves carry energy down the channel from the point of forcing, and that the standing waves do not. Although this is obvious, we may check this assertion by forming a mechanical energy equation. The original equations are

(2.96) $\vec{u}_t + 2\vec{\Omega} \times \vec{u} = -\nabla P - \rho g \hat{k}$,

(2.97) $\rho_t - \frac{N^2 W}{g} = 0$, and

(2.98) $\nabla \cdot \vec{u} = 0$, with the boundary conditions

(2.99) $V = 0$ at $y = 0, L$,

(2.100) $W = 0$ at $z = 1$, and

(2.101) $W = sV$ at $z = sY$.

Forming the dot product of $\vec{u}$ with all the terms of (2.96) we obtain

(2.102) $\frac{1}{2} \frac{\partial}{\partial t} (\vec{u} \cdot \vec{u}) = -\nabla \cdot (p\vec{u}) - \frac{1}{2} \left(\frac{g}{N}\right)^2 \frac{\partial}{\partial t}(\rho^2)$.

The terms on the right hand side of 2.102 were obtained with the help of 2.97 and 2.98. Rearranging 2.102, we write

$$(2.103)\quad \frac{\partial}{\partial t}\left[\frac{|\vec{u}|^2}{2}+\left(\frac{g}{N}\right)^2\frac{\rho^2}{2}\right]=-\nabla\cdot(p\vec{u})$$

The term on the left is the time rate of change of kinetic and potential energy, and the term on the right represents the divergence of energy flux. By integrating 2.103 over planes $x =$ constant, we obtain a statement of the mean energy balance across these planes:

$$(2.104)\quad \int_{y=0}^{L}\int_{z=sy}^{H}\frac{\partial}{\partial t}\left[\frac{|\vec{u}|^2}{2}+\left(\frac{g}{N}\right)^2\frac{\rho^2}{2}\right]dy\,dz=-\int_{y=0}^{L}\int_{z=sy}^{H}(\nabla\cdot p\vec{u})\,dy\,dz$$

We define the symbol $\langle\ \rangle$, with $\int_{y=0}^{L}\int_{z=sy}^{H}\phi\,dy\,dz=\langle\phi\rangle$, to write

$$(2.105)\quad \frac{\partial}{\partial t}\langle E\rangle=-\langle\nabla\cdot p\vec{u}\rangle$$

. E is the total energy, kinetic plus potential. The right hand side of 2.105 is evaluated as follows:

We have $\nabla\cdot p\vec{u}=\frac{\partial}{\partial x}pu+\frac{\partial}{\partial y}pv+\frac{\partial}{\partial z}pw$,

and $\int_{z=sy}^{H}\left(\frac{\partial}{\partial x}pu+\frac{\partial}{\partial y}pv+\frac{\partial}{\partial z}pw\right)dz=$

$$(2.106)\quad \frac{\partial}{\partial x}\int_{z=sy}^{H}pu\,dz+\frac{\partial}{\partial y}\int_{z=sy}^{H}pv\,dz+spv\Big|_{z=sy}-pw\Big|_{z=sy}$$

The bottom boundary condition (2.101) states that $W = SV$ at $Z = Sy$, hence the last two terms in 2.106 cancel. The right hand side of 2.105 is then

$$(2.107)\quad -\langle \nabla \cdot P\vec{u} \rangle = \int_{y=0}^{L} \left[\frac{\partial}{\partial x} \int_{Z=Sy}^{H} Pu\,dZ + \frac{\partial}{\partial y} \int_{Z=Sy}^{H} PV\,dZ \right] dy .$$

Now $\int_{y=0}^{L} \left(\frac{\partial}{\partial y} \int_{Z=Sy}^{H} PV\,dZ \right) dy = \left[\int_{Z=Sy}^{H} PV\,dZ \right] \Big|_{y=0}^{L}$ which is zero, since $V=0$ at $y=0, L$ for all Z. The energy equation is then

$$(2.108)\quad \frac{\partial}{\partial t} \langle E \rangle + \frac{\partial}{\partial x} \langle PU \rangle = 0.$$

If $\frac{\partial}{\partial x} \langle PU \rangle$ (the divergence of energy flux) is zero, then energy cannot increase or decrease in time across planes $x =$ constant. For our wavemaker problem, this means that energy does not propagate down the channel, and would correspond to the case where the wavemaker does not transfer mean energy to the fluid. We will compute the energy flux of the various wave motions after we transform 2.108 to the (x, y, η) coordinate system. Non-dimensionally,

$$\begin{aligned} \langle [PU](x,y,Z) \rangle &= \int_{y=0}^{1} \int_{Z=\epsilon y}^{1} [PU](x,y,Z)\,dZ\,dy \\ &= \int_{y=0}^{1} \int_{\eta=0}^{1} [PU](x,y,\eta) \frac{\partial Z}{\partial \eta} d\eta\,dy \\ &= \int_{y=0}^{1} (1-\epsilon y) \left[\int_{\eta=0}^{1} [PU](x,y,\eta)\,d\eta \right] dy . \end{aligned}$$

The mean energy flux in the (x,y,η) system is then

$$(2.110)\quad \langle PU\rangle - \epsilon\int_{y=0}^{1} y\left[\int_{\eta=0}^{1} PU\,d\eta\right] dy \quad ,$$

where $\langle\ \rangle$ now implies integration over the plane bounded by $y=0,1$ and $\eta=0,1$. For the flat-bottom channel, $\epsilon=0$ and $\eta=z$.

(i) Flat-Bottom Kelvin Waves

$$PU = \frac{C_i^2 k_1}{\sigma} e^{-\frac{2k_1 f}{\sigma} y} \cos^2 \pi z \cos^2(k_1 x-\sigma t)$$

and

$$(2.111)\quad \langle PU\rangle = \frac{C_i^2 k_1}{\sigma} \cos^2(k_1 x-\sigma t)\int_{y=0}^{1}\int_{z=0}^{1} e^{-\frac{2k_1 f}{\sigma} y} \cos^2 \pi z\, dy\,dz \quad .$$

Upon performing the y -integration, we have

$$(2.112)\quad \langle PU\rangle = \frac{C_i^2}{2f} \cos^2(k_1 x-\sigma t)\left(1-e^{-\frac{2k_1 f}{\sigma}}\right)\int_{z=0}^{1} \cos^2 \pi z\, dz \quad ,$$

and finally,

$$(2.113)\quad \langle PU\rangle = \frac{C_i^2}{4f} \cos^2(k_1 x-\sigma t)\left(1-e^{-\frac{2k_1 f}{\sigma}}\right) \quad , \text{ and}$$

$$(2.114)\quad \frac{\partial}{\partial x}\langle PU\rangle = \frac{-2k_1 C_i^2}{4f} \sin(k_1 x-\sigma t)\cos(k_1 x-\sigma t)\left[1-e^{-\frac{2k_1 f}{\sigma}}\right].$$

We see that $\frac{\partial}{\partial x}\langle PU\rangle \neq 0$ and energy propagates down the channel

away from the wavemaker.

(ii) Flat-Bottom Standing Oscillations

(χ-decaying)

For the low frequency case ($\sigma << f$, $\sigma << N$), PU is

$$\sim e^{2\gamma x} \cos^2 \pi z \sin n\pi y \cos n\pi y \sin^2 \sigma t \ .$$

Then $$\langle PU \rangle \sim \int_0^1 \cos^2 \pi z \int_0^1 \sin n\pi y \cos n\pi y \, dy \, dz$$

which is zero. Since the energy flux is zero, no energy propagates down the channel.

(iii) Bottom-Trapped Waves

$PU \sim \sin n\pi y \cos n\pi y \cosh^2 \mu_n (\eta - 1) e^{2i(kx - \sigma t)}$, and the mean energy flux is

$$(2.115) \quad \langle PU \rangle = \int_{y=0}^{1} \int_{\eta=0}^{1} \sin n\pi y \cos n\pi y \cosh^2 \mu_n (\eta - 1) e^{2i(kx - \sigma t)} \, dy \, d\eta$$

$$- \epsilon \int_{y=0}^{1} y \left[\int_{\eta=0}^{1} \sin n\pi y \cos n\pi y \cosh^2 \mu_n (\eta - 1) \, e^{2i(kx - \sigma t)} \, d\eta \right] dy \ .$$

The first integral is zero, but the second is $O(\epsilon)$. The energy flux divergence is also $O(\epsilon)$ and this is due to the fact that the group velocity associated with low frequency oscillations is in general a small quantity.

Summary of the Results

In a semi-infinite channel (Figure 1) whose fluid is forced by a wavemaker at one end, the following oscillatory motions are possible:

Flat-Bottom

(1) Standing Oscillations, trapped to the wavemaker, with no net phase or energy propagation. The motion serves to provide continuity between the fluid and the wavemaker. If the wavemaker puts no net energy into the fluid, the standing waves serve to insulate the forcing from the main body of fluid since the amplitude of the motion decays rapidly away from the wavemaker.

(2) Baroclinic Internal Kelvin Waves. These arise when the wavemaker motion is non-symmetric in the cross-channel coordinate y, i.e., $\int_{y=0}^{L} u_{wm}\, dy \neq 0$, and mean energy is put into the fluid. The waves propagate (both phase and energy) down the channel and are trapped against the $y=L$ sidewall by rotation.

Sloping Bottom

(1) The Standing Oscillations of the flat-bottom case now have phase propagation down the channel, but are still trapped to the wavemaker and cannot transport energy down the channel.

(2) Topographic Oscillations with vertical structure $\cosh \frac{KHN}{F}(\eta-1)$.

These are:

(i) Topographic Rossby waves if $\frac{HN}{fL} << 1$ and $\sigma \geq sN$, and

(ii) Bottom-trapped waves if $\frac{HN}{fL} \geq 1$ and $\sigma < sN$. These decay exponentially away from the bottom in a length of $O(\frac{fL}{HN})$ and have westward components of phase and group velocity.

(3) The Baroclinic Kelvin Waves of the flat-bottom case are virtually unchanged. The cross-channel (y) velocity component is zero and the fluid particles do not cross planes of constant fluid height when the bottom becomes sloped. The Kelvin waves have large $(O(\frac{1}{\epsilon}))$ down-channel wavelength.

Chapter III The Wavemaker Problem

Now that we know the possible modes, this chapter will outline the wavemaker problem -- matching the fluid modes to an arbitrary forcing function at $x = 0$.

The problem involves matching the x-velocity of the fluid to the x-velocity of the wavemaker (at the wavemaker), and is made tractable by linearizing the wavemaker motion so that the matching takes place at $x = 0$.

Let ξ be the x-displacement of the wavemaker. (See Figure 17.) The inviscid fluid in contact with the paddle also has this displacement; therefore, the x-component of the fluid velocity (u_f) at the wavemaker is given by

$$(3.1) \qquad u_f = \frac{d\xi}{dt} = \xi_t + V\xi_y + W\xi_z \quad .$$

If we scale ξ by a (the particle excursion in the x-y plane), V by $a\sigma$ (σ is the paddle frequency), and W by $a_v\sigma$ (a_v is the particle excursion in the x-z plane), 3.1 becomes

$$(3.2) \qquad a\sigma u_f^* = a\xi_t^* + a^2\sigma V^*\xi_y^* + aa_v\sigma W^*\xi_z^* \quad .$$

The $(*)$ superscript denotes non-dimensional variables. If we further scale t by $\frac{1}{\sigma}$, (x, y) by $\frac{1}{\ell}$ (the horizontal scale of the motion), and z by $\frac{1}{m}$ (the vertical scale of the motion), 3.2 becomes (dropping $*$'s)

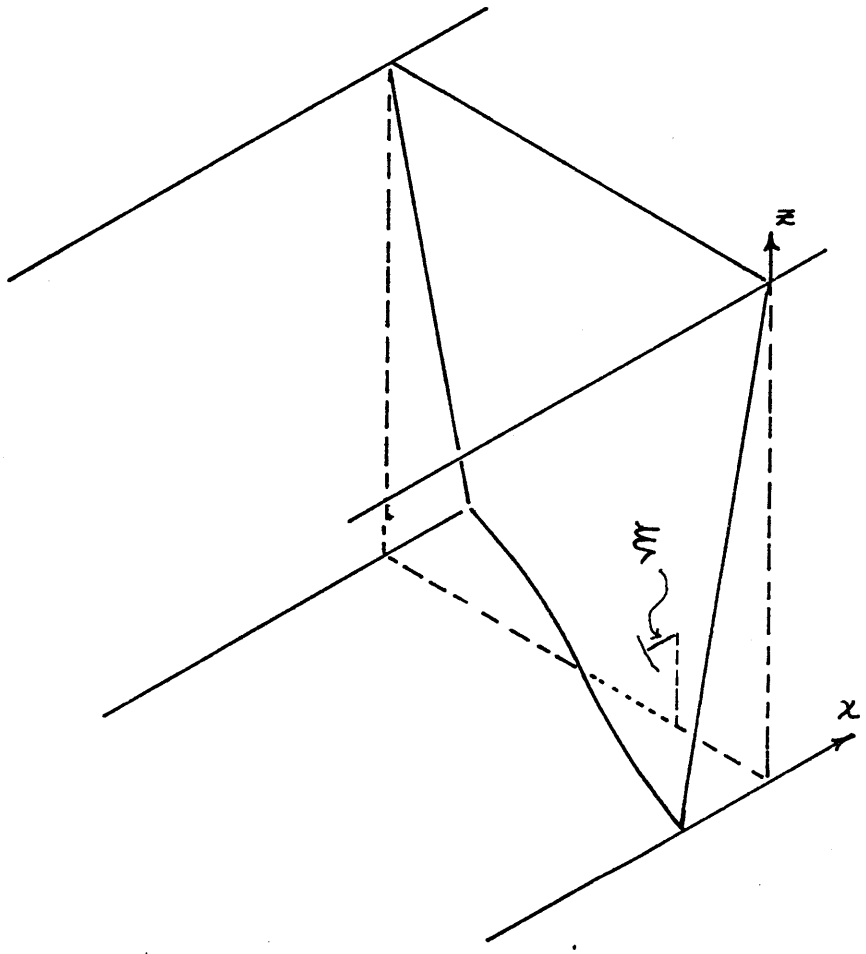

Figure 17.

The wavemaker.

$$(3.3)\quad a\sigma u_f = a\sigma \xi_t + a^2 \sigma \ell V \xi_y + a a_v \sigma m W \xi_z \ ,$$

or,

$$(3.4)\quad u_f = \xi_t + a\ell V \xi_y + a_v m W \xi_z \ .$$

Expanding the left hand side of 3.4 in a Taylor series about $\chi = 0$, we find

$$(3.5)\quad u_f(\chi=0) = (a\ell)\frac{\partial u_f}{\partial \chi}(\chi=0) + \cdots =$$

$$\xi_t + a\ell V \xi_y + a_v m W \xi_z \ .$$

Then if $a\ell \ll 1$, and $a_v m \ll 1$, we perform the matching at $\chi = 0$ and write

$$(3.6)\quad u_f(\chi=0) = \xi_t \ .$$

The available fluid modes are (for $\sigma \leq SN$, and at $\chi = 0$) Kelvin:

$$(3.7)\quad {}^{K}u_k \begin{Bmatrix} \gamma_k \\ \gamma_k' \end{Bmatrix} e^{-\frac{k_x f}{\sigma} y} \cos k\pi\eta \begin{Bmatrix} \cos\sigma t \\ \sin\sigma t \end{Bmatrix} \ .$$

Note: We allow energy to propagate only away from the forcing, because

the channel is infinitely long. Since the group velocity has the sign of the phase speed, we must keep $\frac{\sigma}{k_n} < 0$.

Bottom-Trapped:

$$(3.8)\quad {}^{B}u_n = \begin{Bmatrix} \beta_n \\ \beta'_n \end{Bmatrix} \cos n\pi y \cosh \mu_n(\eta-1) \begin{Bmatrix} \cos\sigma t \\ \sin\sigma t \end{Bmatrix} \quad , \text{ and}$$

χ-decaying standing waves

$$(3.9)\quad {}^{H}u_{n\lambda} = \alpha_{n\lambda} \cos n\pi y \left(\cosh a_{n\lambda}(\eta-1) \cos b_{n\lambda}(\eta-1) \cos\sigma t + \sinh a_{n\lambda}(\eta-1) \sin b_{n\lambda}(\eta-1) \sin\sigma t \right)$$

We match these χ-velocity modes (summing over λ and n) to the wave-maker, $u_{wm} = \xi_t$.

If we write

$$(3.10)\quad u_{wm} = \xi_t = Re\{ U(y,z) e^{i\sigma t} \} \quad ,$$

then

$$(3.11)\quad u_{wm} = U(y,z) \cos\sigma t + U'(y,z) \sin\sigma t \quad .$$

We then rewrite 3.4, 3.5, 3.6 to obtain

$$(3.12)\quad {}^{K}U_k = F_k(y)\,\cos k\pi\eta\,(\gamma_k \cos\sigma t + \gamma_k' \sin\sigma t)\,,$$

$$(3.13)\quad {}^{B}U_n = G_n(\eta)\,\cos n\pi y\,(\beta_n \cos\sigma t + \beta_n' \sin\sigma t)\,,\ \text{and}$$

$$(3.14)\quad {}^{H}U_{nk} = \alpha_{nk}\,\cos n\pi y\,(H_{nk}(\eta)\cos\sigma t + I_{nk}(\eta)\sin\sigma t)\,.$$

σ is fixed by the wavemaker frequency, and the matching becomes:

$$(3.15)\quad U(y,z) = \sum_k \gamma_k F_k(y)\cos k\pi\eta + \sum_n \beta_n G_n(\eta)\cos n\pi y + \sum_k \sum_n \alpha_{nk} H_{nk}(\eta)\cos n\pi y\,,\ \text{and}$$

$$(3.16)\quad U'(y,z) = \sum_k \gamma_k' F_k(y)\cos k\pi\eta + \sum_n \beta_n' G_n(\eta)\cos n\pi y + \sum_k \sum_n \alpha_{nk} I_{nk}(\eta)\cos n\pi y\,.$$

The wavemaker is constrained by a no-net mass flux condition:

$$(3.17)\quad \int_{y=0}^{'} \int_{\eta=0}^{'} \begin{Bmatrix} U \\ U' \end{Bmatrix} dy\,d\eta = 0.$$

The fluid is similiarly constrained, and we see that each mode does indeed satisfy 3.17.

By writing

$$(3.18)\quad \begin{Bmatrix} U(y,\eta) \\ U'(y,\eta) \end{Bmatrix} = \sum_{n=1}^{\infty} \cos n\pi y \left[\begin{Bmatrix} D_{n0} \\ D'_{n0} \end{Bmatrix} + \sum_{s=1}^{\infty} \begin{Bmatrix} D_{ns} \\ D'_{ns} \end{Bmatrix} \cos s\pi\eta \right]$$

$$+ \sum_{s} \cos s\pi\eta \left[\begin{Bmatrix} E_{0s} \\ E'_{0s} \end{Bmatrix} + \sum_{n} \begin{Bmatrix} E_{ns} \\ E'_{ns} \end{Bmatrix} \cos n\pi y \right] ,$$

we decompose the paddle motion into a complete orthogonal set and satisfy 3.17. We now expand F, G, H, I in complete orthogonal sets $\left\{1, \cos g\pi\left(\frac{y}{\eta}\right)\right\}$, and equate cosine coefficients of the fluid and the wavemaker to perform the matching. Expanding the fluid set, we have

$$(3.19)\quad {}^{A}U_{ns} = \alpha_{ns} \cos n\pi y \left[\left(a_{ns0} + \sum_{g} a_{nsg} \cos g\pi\eta \right) \cos\sigma t \right.$$

$$\left. + \left(a'_{ns0} + \sum_{g} a'_{nsg} \cos g\pi\eta \right) \sin\sigma t \right] ,$$

$$(3.20)\quad {}^{B}U_{n} = \cos n\pi y \left[b_{n0} + \sum_{g} b_{ng} \cos g\pi\eta \right] \times$$

$$\left[\beta_n \cos\sigma t + \beta'_n \sin\sigma t \right] , \text{ and}$$

$$(3.21)\quad {}^{K}U_{s} = \cos g\pi\eta \left[C_{0g} + \sum_{r} C_{rg} \cos r\pi y \right] \times$$

$$\left[\gamma_g \cos\sigma t + \gamma'_g \sin\sigma t \right] .$$

Performing the matching (3.15, 3.16) using 3.18, we have

$$(3.22)\quad \sum_s \alpha_{ns}\, a_{ns0} + \beta_n b_{n0} = D_{n0} \quad ,$$

$$(3.23)\quad \gamma_q C_{0q} = E_{0q} \quad ,$$

$$(3.24)\quad \sum_s \alpha_{ns}\, a_{nsq} + \beta_n b_{nq} + \gamma_q C_{nq} = D_{nq} + E_{nq} \, .$$

$$(3.25)\quad \sum_s \alpha_{ns} a'_{ns0} + \beta'_n b_{n0} = D'_{n0} \quad ,$$

$$(3.26)\quad \gamma'_q C_{0q} = E'_{0q} \quad ,$$

$$(3.27)\quad \sum_s \alpha_{ns}\, a'_{nsq} + \beta'_n b_{nq} + \gamma'_q C_{nq} = D'_{nq} + E'_{nq} \, .$$

3.22 - 3.24 are the result of matching the $\cos \sigma t$ dependence while 3.25 - 3.27 are the result of matching the $\sin \sigma t$ dependence.

We see that by choosing a wavemaker whose mean cross-channel motion is zero, i.e., $\int_0^{'} \begin{Bmatrix} U \\ U' \end{Bmatrix} dy = 0$ then $E_{0q} = E_{nq} = 0$, and no Kelvin waves are excited. Upon making this selection, the matching problem becomes:

$$(3.28)\quad \sum_s \alpha_{ns}\, a_{ns0} + \beta_n b_{n0} = D_{n0}$$

$$\sum_s \alpha_{ns}\, a_{nsq} + \beta_n b_{nq} = D_{nq}$$

$$(3.29)\quad \sum_{s} \alpha_{ns}\, a'_{ns0} + \beta'_{n}\, b_{n0} = D'_{n0}$$

$$\sum_{s} \alpha_{ns}\, a'_{nsq} + \beta'_{n}\, b_{nq} = D'_{nq}$$

Rewriting 3.28 and 3.29 in matrix form, we have

$$\begin{bmatrix} D_{n0} \\ D_{n1} \\ D_{n2} \\ \vdots \end{bmatrix} = \begin{bmatrix} b_{n0} & a_{n00} & a_{n10} & \cdots \\ b_{n1} & a_{n01} & a_{n11} & \cdots \\ b_{n2} & a_{n02} & a_{n12} & \cdots \\ \vdots & \vdots & \vdots & \end{bmatrix} \begin{bmatrix} \beta_n \\ \alpha_{n0} \\ \alpha_{n1} \\ \vdots \end{bmatrix}$$

, and

$$\begin{bmatrix} D'_{n0} \\ D'_{n1} \\ D'_{n2} \\ \vdots \end{bmatrix} = \begin{bmatrix} b_{n0} & a'_{n00} & a'_{n10} & \cdots \\ b_{n1} & a'_{n01} & a'_{n11} & \cdots \\ b_{n2} & a'_{n02} & a'_{n12} & \cdots \\ \vdots & \vdots & \vdots & \end{bmatrix} \begin{bmatrix} \beta'_n \\ \alpha_{n0} \\ \alpha_{n1} \\ \vdots \end{bmatrix}$$

In the matching matrices, the number of rows is determined by the number of cross-channel (n) modes and the number of vertical (q) modes, while the number of columns is determined by the number of complex μ (s) modes. If actually solving for α , β and β', we truncate the matching matrices at a finite number of modes, then perform the inversion operations. The actual calculation of the matching will not be done here, as we are merely interested in isolating the purely bottom-trapped waves for laboratory study, and this is quite easily done since the complex μ modes decay rapidly away from the wavemaker.

Chapter IV Proposed Laboratory Experiment

In designing a laboratory experiment to isolate and study bottom-trapped waves in a salt-stratified fluid, several factors must be considered. For example, we have seen that we must have $\sigma < SN$ in order to excite the bottom-trapped waves.

The general plan is to construct a long channel with a wavemaker in one end. (Figure 18.) The frequency and amplitude of the fluid motion is fixed by the wavemaker. The wavemaker motion will be symmetric in the cross-channel coordinate, hence no Kelvin waves will be excited. As long as $\frac{\sigma}{SN}$ is less than 1, both the purely bottom-trapped (real μ) modes and the standing (complex μ) modes are produced. The bottom-trapped waves propagate to the left of an observer who is facing shallow water, hence the wavemaker must be installed in the end of the channel which is to the right of an observer who is looking up the slope. The bottom-trapped waves should be easily isolated from the complex μ waves since the latter are trapped to the wavemaker.

In choosing the stratification and rotation, we must consider the subtle flow induced when constant density surfaces terminate on sloping boundaries. In a rotating experiment, the constant density surfaces (isopycnals) are paraboloids, and therefore intersect vertical boundaries at some angle ϕ (see Figure 19). This implies that a density gradient $\frac{\partial \rho}{\partial r}$ (r is the radial coordinate in the rotating system) exists on planes of constant depth, i.e., planes perpendicular to gravity, particularly at the sidewall. If the boundaries are insulated (true for salt stratification),

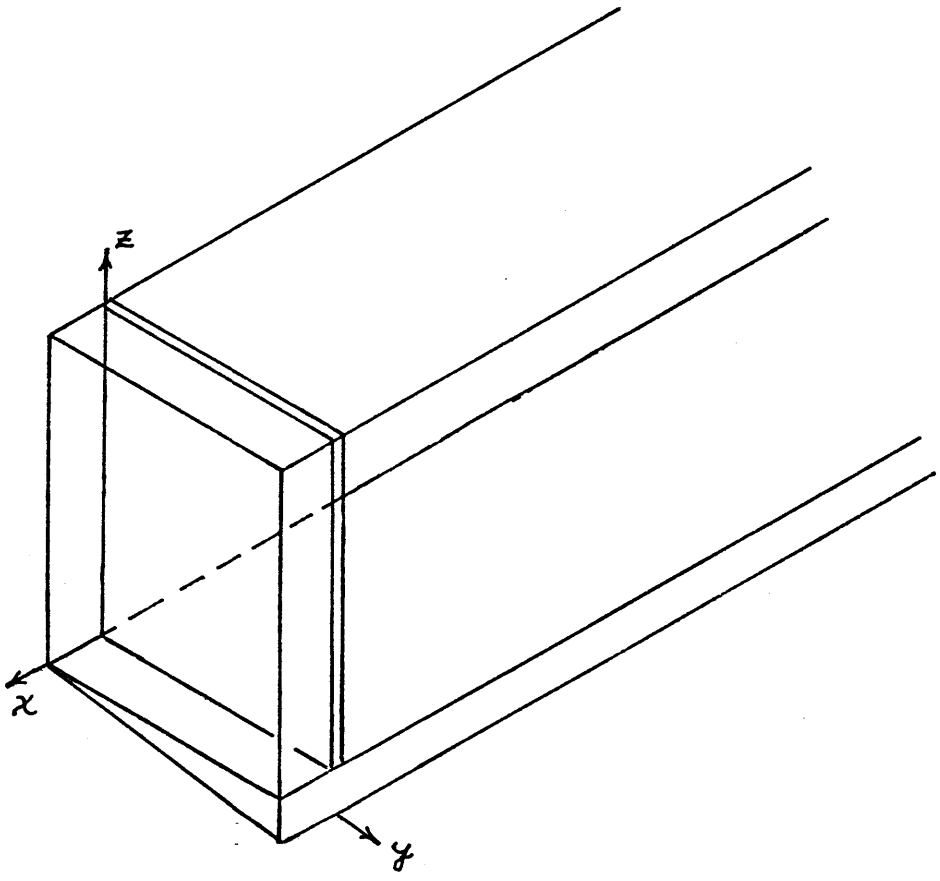

Figure 18.

Geometry of the channel with wavemaker installed.

the density gradient cannot drive salt through the wall, and a flow is induced along the wall which adjusts the isopycnals in such a way that the radial density gradient vanishes at the wall. Under laboratory conditions the magnitude of this flow is very small ($O(\frac{\Omega^2 L}{g'})$ where L is the radius of the container, and g' is the buoyancy-reduced gravity. We must consider this flow if the magnitude of the flow under study is also small.

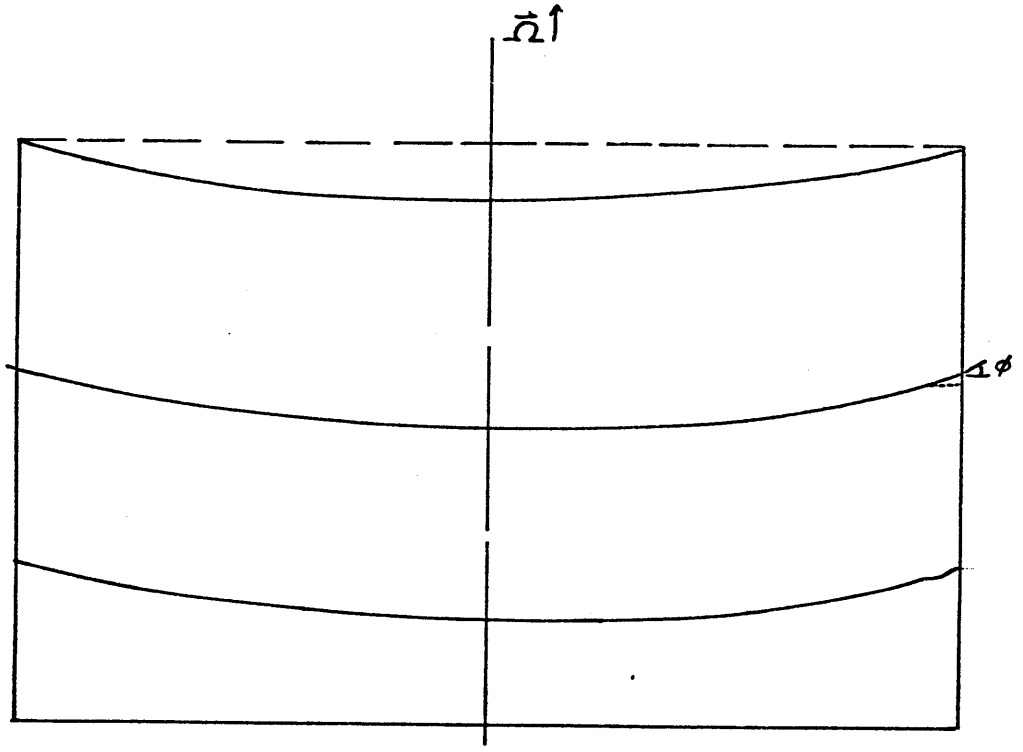

Figure 19.

Isopycnals in a rotating cylinder.

Obviously, a semi-infinite channel cannot be constructed; however, the channel will be made as long as possible, subject to the limitations of turntable capacity, plexiglass strength and the size of the laboratory. It is hoped that viscous damping will insure that the waves do not reach the end of the channel opposite the forcing so that the idealized wavemaker problem will be approached. The sloping bottom is made up of machined plexiglass wedges of slope S, hence S can be no smaller than that which can accurately be machined.

We wish to optimize the "observability" of the waves so we will select parameters of f, N, L and H such that the resulting group velocity and vertical e-folding length of the bottom-trapped motion tend to enhance detection, and at the same time insure that the standing modes decay rapidly away from the wavemaker. The horizontal e-folding decay length of the standing modes is never more than $\frac{L}{\pi}$ (see Figure 5). This means that the complex μ (standing) modes and the real μ (bottom-trapped) modes are easily separated, since the latter are freely propagating down the channel.

We will also need to estimate the horizontal viscous decay length of the wave motion for two reasons: (1) as previously stated, we desire that the motion be completely damped before it reaches the end of the channel, and (2) we don't want the motion damped out by viscosity before it can be easily observed.

Finally, we must have $R_0 \equiv \frac{U}{fL} \ll 1$, $E \equiv \frac{\nu}{fL^2} \ll 1$, and $\epsilon \equiv \frac{SL}{H} \ll 1$ in order to utilize the small slope, linear and inviscid theory of Chapter 2. In addition, the low frequency limit may be approached by insuring that $\delta \equiv \frac{\sigma}{f} \ll 1$.

The above important parameters -- frequency (σ), down-channel group velocity (C_{gk}), vertical e-folding length (λe), and horizontal viscous decay length (D_L) of the bottom-trapped waves are now discussed in detail.

Beginning with the bottom-trapped wave dispersion relation, we have:

$$(4.1)\quad \sigma = \frac{sNk_n}{K_n} \coth \frac{K_n NH}{f} \quad , \text{where } K_n \equiv (l_n^2 + k_n^2)^{1/2}, \; l_n = \frac{n\pi}{L}.$$

For convenience, we set $k_n = \alpha l_n$.

Then $$\sigma = \frac{\alpha \Delta N}{\sqrt{1+\alpha^2}} \coth\left[(1+\alpha^2)^{1/2} \frac{n\pi}{L} \frac{HN}{f}\right].$$

This may be approximated as $\sigma \cong \frac{\alpha SN}{\sqrt{1+\alpha^2}}$ provided that the $\coth$ argument is $\gtrsim 1$.

The group velocity is

$$(4.2)\quad C_{gk} = \frac{\partial \sigma}{\partial k} = \frac{SN}{K^2}\left(\frac{l^2}{K} \coth \frac{KHN}{f} + \frac{HN}{f} k^2 \operatorname{csch}^2 \frac{KHN}{f}\right),$$

and if $k_n = \alpha l_n$, then

$$(4.3)\quad C_{gk} = \frac{SN}{K^3} l^2 \left(\coth \frac{KHN}{f} + \alpha^2 \frac{KHN}{f} \operatorname{csch}^2 \frac{KHN}{f}\right).$$

Both $\coth \frac{KHN}{f}$ and $\alpha^2 \frac{KHN}{f} \operatorname{csch}^2 \frac{KHN}{f}$ are plotted in Figure 20 for two values of α.

We see that the second term of 4.3 may be neglected if $\frac{KHN}{f} \gg 1$, and that

$$(4.4)\quad C_{gk} \cong \frac{SN\left(\frac{L}{n\pi}\right)}{(1+\alpha^2)^{3/2}}$$

The vertical e-folding length of the motion is given by

$$\lambda_{ne} \equiv \frac{1}{\mu_n} = \frac{f}{N}\left(k_n^2 + \ell_n^2\right)^{-1/2}$$

With $k_n = \alpha \ell_n$, this becomes

$$(4.5)\quad \lambda_{ne} = \frac{f}{N}\left(\frac{L}{n\pi}\right)(1+\alpha^2)^{-1/2} \quad .$$

The percent (of channel depth) e-folding length is $\frac{\lambda_{ne}}{H}$.

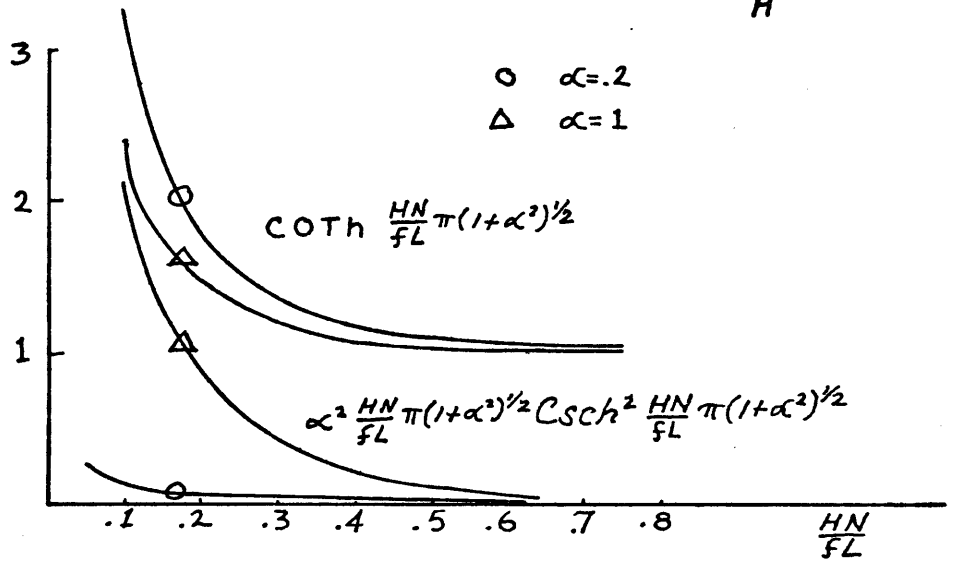

Figure 20.

Relative sizes of $\coth \frac{KHN}{f}$ and $\alpha^2 \frac{KHN}{f} \operatorname{csch}^2 \frac{KHN}{f}$

An estimate of the horizontal viscous decay length for the bottom-trapped waves may be obtained by considering the classical homogeneous spin-down time, $\Omega^{-1} E^{-1/2}$ (E is the Ekman number, $(\frac{\nu}{fL^2})$).

(4.6) $T_d \equiv \Omega^{-1} E^{-1/2} = \frac{2}{f}\left(\frac{\nu}{fh^2}\right)^{-1/2}$, where ν is the kinematic viscosity. h is the vertical scale of the motion and is to be approximated by $\frac{1}{\mu} = \lambda_e$.

Thus

(4.7) $T_d = \frac{2\lambda_e}{\sqrt{\nu f}} = \frac{2}{\sqrt{\nu f}}\left(\frac{L}{n\pi}\right)\frac{f}{N}(1+\alpha^2)^{-1/2}$,

and the viscous decay length is then

(4.8) $D_L = T_d \cdot C_{gk} = 2S\sqrt{\frac{f}{\nu}}\left(\frac{L}{n\pi}\right)^2(1+\alpha^2)^{-2}$.

In summary, we have the following important experimental parameters:

(i) $\sigma = \frac{\alpha}{(1+\alpha^2)^{1/2}} SN$

(ii) $C_{gk} = \frac{SN(\frac{L}{n\pi})}{(1+\alpha^2)^{3/2}}$

(iii) $\lambda_e = \frac{f}{N}\left(\frac{L}{n\pi}\right)\frac{1}{(1+\alpha^2)^{1/2}}$

(iv) $D_L = 2\sqrt{\frac{f}{\nu}}\left(\frac{L}{n\pi}\right)^2 S \frac{1}{(1+\alpha^2)^2}$

Several values of the above for $n=1$ (first cross-channel mode) and $\alpha = 0-1$ were computed, and the results are plotted in Figure 21. Fixing the channel parameters to $S=.1$ and $L=25cm$, and setting $\nu = .01\ cm^2/sec$, we have for $\alpha = 1/2$:

$$\sigma \cong .045N\ (sec^{-1}), \quad C_{gk} \cong .56N\ (cm/sec),$$

$$\lambda_e \cong 7.13\frac{f}{N}\ (cm) \quad \text{and} \quad D_L \cong 81.3\sqrt{f}\ (cm)$$

For a first experiment, we set $f=1$ and $N=2$, yielding $\sigma \cong .09/sec$ $C_{gk} \cong 1.1\frac{cm}{sec}$, $\lambda_e \cong 3.5cm$, and $D_L \cong 81.3\ cm$.
If the paddle excursion is $6cm$, the maximum paddle velocity is $4\cdot(6cm)\cdot\sigma = 2.16\frac{cm}{sec}$, and the Rossby number for this speed is $\sim .04$.

Notes On The Experimental Apparatus

A 2m x 50 cm x 25 cm plexiglass channel was constructed, and eight wedges of slope $S = 0.1$ were machined for the sloping bottom. The channel is mounted on aluminum I-beams which are attached to the ultra-stable air bearing turntable designed by Saunders and Beardsley (1972). The rotation period is monitored by a magnetic reed switch connected to a digital counter.

The wavemaker consists of a rubber sheet held fixed from the fluid surface to mid-depth, with linearly increasing amplitude toward the channel bottom. The paddle frequency is adjustable by means of a Bodine Speed

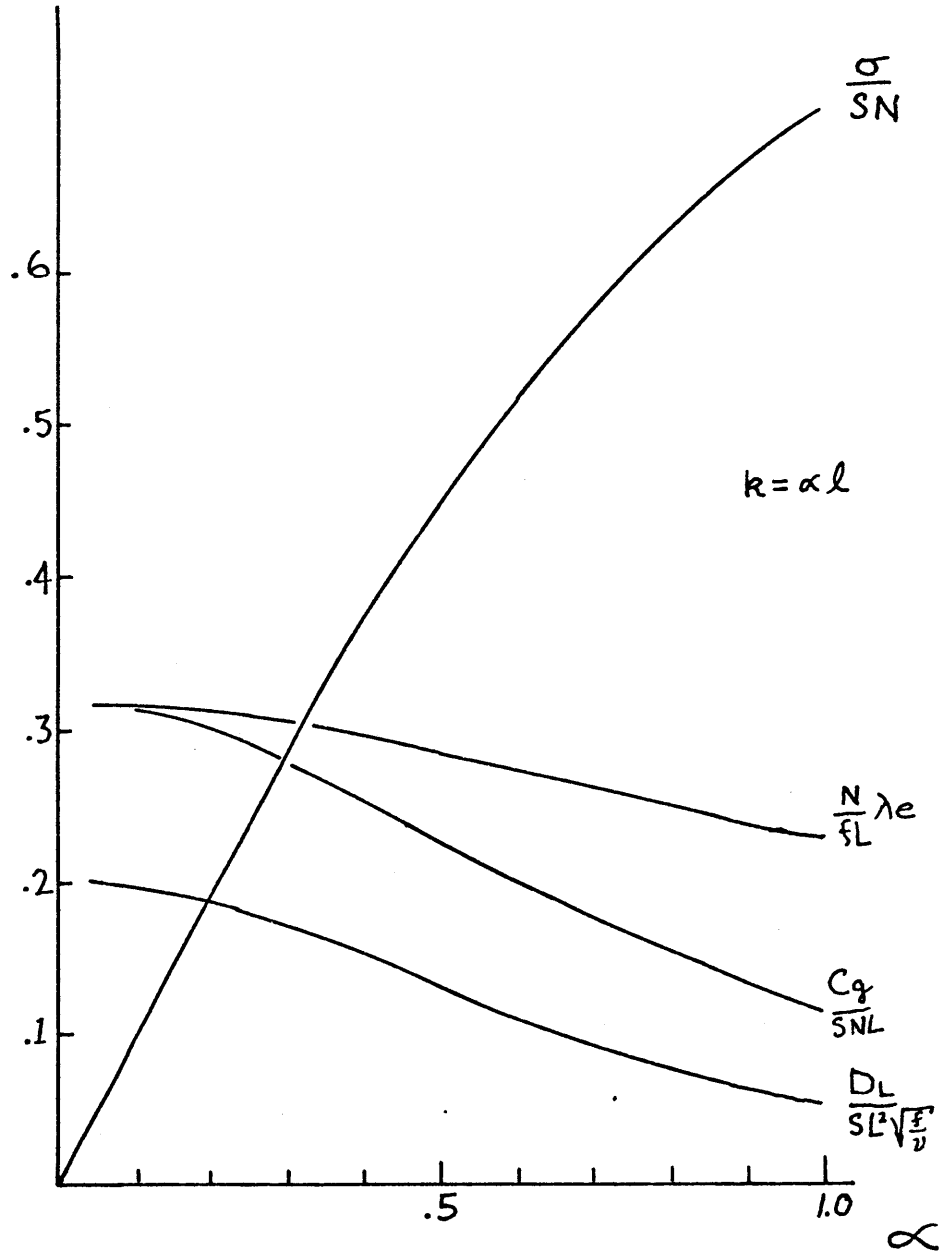

Figure 21.

Parameters of the first ($n=1$) bottom-trapped mode.

control motor.

The channel is linearly stratified by the method of Oster (1965) while rotating to speed up the fluid equilibrium process with less mixing. The density gradient is monitored by a continuous output, vertically-tracked conductivity probe. The results of these conductivity "casts" are displayed on an X-Y recorder.

Visualizing The Flow

Baker's (1966) thymol blue technique is perhaps the most precise method of measuring small fluid velocities, but it is not very practical here, due to the great quantity of fluid involved (in excess of 70 gallons).

Commercially available adjustable-density polystyrene beads cannot be adjusted to the required density of $\sigma_t > 50$ ($\sigma_t \equiv [\rho - 1] \times 10^3$), as the beads have a maximum density of $\sigma_t \sim 30$. A technique of manufacturing neutrally buoyant floats is now being perfected in which molten paraffin is mixed with metal powder to produce beads with the desired buoyancy. These floats would be inserted in the channel (during filling) at various depths, then photographed to reveal wavelengths, trapping lengths and fluid velocities.

REFERENCES

Baker, D. J. (1966) A Technique for the Precise Measurement of Small Fluid Velocities, Jour. Fluid Mech., 26, 573-575.

Oster, G. (1965) Density Gradients, Sci. Amer., 213(2), 70-76.

Phillips, N. A. (1957) A Coordinate System Having Some Special Advantages for Numerical Forecasting, Jour. Meteor., 14, 184-185.

Rhines, P. B. (1970) Edge-, Bottom-, and Rossby Waves in a Rotating Stratified Fluid, Geophys. Fl. Dyn., I, 173-302.

Riser, S. C. (1974) Observations of Mesoscale Eddies over Rough Topography in the Western North Atlantic, S.M. Thesis, M.I.T.

Saunders, K.D., and R. C. Beardsley (1972) The Design and Construction of an Ultra-Stable Air-Bearing Turntable, Rev. Sci. Inst., 43(10), 1451-1453.

Suarez, A. A. (1971) The Propagation and Generation of Topographic Oscillations in the Ocean, Ph.D. Thesis, M.I.T.- W.H.O.I.